# ADSORPTION AND ORIENTATION ANALYSIS OF *p*-NITROPHENOLATE AT AIR/AQUEOUS INTERFACES

**A THESIS**

**SUBMITTED TO THE GRADUATE SCHOOL**

**IN PARTIAL FULFILLMENT OF THE REQUIREMENTS**

**FOR THE DEGREE OF**

**MASTER OF SCIENCE**

**BY**

**RYAN YOUNG**

**DR. MAHAMUD SUBIR – ADVISOR**

**BALL STATE UNIVERSITY**

**MUNCIE, INDIANA**

**JULY 2017**

## Acknowledgment

I would like to begin by thanking Ball State University and the Department of Chemistry for giving me the opportunity to learn and gain experience. Without such resources and all the people working to provide me with excellent guidance and education throughout this endeavor I could not have accomplished what I have within these past two years.

I would like to thank my advisor Dr. Mahamud Subir. I learned so much under your mentorship. This learning was not confined to science but also in things such as history, philosophy, and character. It was inspiring to be able to work with someone that was intelligent, thoughtful, tough, and unflinching. You showed me what it takes for success within this community and I thank you.

I would also like to thank my committee, Dr. Li and Dr. Zubkov. You were both very kind and offered me many opportunities to probe deeper in my understanding of my project. I value your insights as well as your aid within my development as a scientist.

Integral not only to my grounding within the culture of the department but also with my learning the new and varied systems within were my group members. I would like to thank Tyler Williams, Mansour Alsarrani, Giada Dalla Pozza, James Adair, Jessica Rizzo, Mehjabeen Khan, and Luke Schumaker.

Finally, I would like to thank Mr. Daniel Headly and Ms. Margret Schmits. Both Maggie and Dan are wonderful people within their own regard. Allowing not only for friendship but they supplied me with knowledge and complementary work. Margret did all of the surface tension measurements essential to giving my work context. Dan taught me how to run the laser as well as laid the ground work for all surface investigation within our lab with his thesis.

# Table of Contents

## List of Figures

# List of Tables

**Page Number**

# List of Equations

# Chapter 1 - Introduction

This thesis depicts the molecular behavior of an aromatic anion, *p*-nitrophenolate (*p*-$NP^-$), at different air/aqueous interfaces. The objective of this study has been to explore the adsorption and molecular orientation of *p*-$NP^-$ at the air/aqueous interface. Furthermore, at these interfaces we investigated the influence of various factors, such as lipid monolayer and electrolyte concentration, on the orientation of the adsorbed *p*-$NP^-$.

In this chapter, the motivations of this project are highlighted and the discussion of different questions addressed in pursuing these research objectives. In chapter 2, experimental techniques, including the theory and application of non-linear spectroscopy, will be discussed. Chapter 3 will cover a series of experiments meant to restrict movement of *p*-$NP^-$ at interfacial regions by additions of monolayers to the air/aqueous interface. Included within this chapter will be the discussion of adsorption isotherms based on analysis of the electric field generated by second harmonic generation. The effects of electrolyte concentration on *p*-$NP^-$ orientation about the surface normal are introduced within Chapter 4. The adsorption of *p*-$NP^-$ will also be conferred in Chapter 4. To summarize the experiments discussed in previous chapters, Chapter 5 will be presented. In addition to summarization, the physical interpretation of data as well as future directions of this project will be discussed within Chapter 5.

## 1.1 Fundamental Motivation

Skepticism and more specifically empiricism are philosophical beliefs of the nature of knowledge. These philosophies question the ability to “know” and how any knowledge may be arrived upon. Empiricism in the vein of such men as Sir Francis Bacon and John Locke is the progenitor of modern science. Such a philosophy puts an emphasis on the building of physical

evidence to discover the nature of reality. Science and empiricism offers a way in which the senses can be used to reveal truth in opposition to mere perceptions. Described by Sir Francis Bacon in his work Novum Organum Scientiarum:

> "Now my method, though hard to practice, is easy to explain; and it is this. I propose to establish progressive stages of certainty. The evidence of the sense, helped and guarded by a certain process of correction, I retain. But the mental operation which follows the act of sense I for the most part reject; and instead of it I open and lay out a new and certain path for the mind to proceed in, starting directly from the simple sensuous perception."[1]

Science as described provides filters of truth to arrive at an authentic objective picture of the physical universe. In this search for truth the natural instrument of rational being's mind combined with instruments to improve one's sensory perception allow for investigation into the nebulous universe and tease out fundamental truths.[2] This search for truth is a corollary of the human condition and stands alone as an essential meaning to physical being.[3-4] Not only as a mode of being does science exist but fundamental science increases our knowledge of specific systems upon which we can model more complex environments that are present within the physical reality we inhabit. Understanding the elementary science of any experimental system is a pivotal point for beginning scientific understanding of myriad systems of overlapping variability. Should the fundamentals be overlooked there is great hazard that increasingly complex systems will be misunderstood and incorrect conclusions or hypotheses will be made. This can at times make fundamental science seem more abstract but it is the pavement upon which utility can be laid.

In the spirit of this discussion, the fundamental understanding we sought was of *p*-$NP^-$ adsorption and orientation at the air/aqueous interface. Knowledge of *p*-$NP^-$ in isolation is a

required stepping stone to adequately build upon such knowledge by adding complexity and modeling real world environments. Knowledge for sake of truth as well as groundwork for more complex systems of *p*-$NP^-$ carry great and inherent value both in interest and in the lifeblood of science. Forces at this interface are not well understood and unique. This presents a niche of investigation that has yet to be performed allowing for characterization of a ubiquitous interfacial region regarding an organic anion.

Fundamentally, ions were classically understood to be void at the air/aqueous interface partly due to anisotropy presented by such interfaces.[5] It was believed because when electrolytes were solvated into water the surface tension of the water increased lending evidence to the idea that ions penetrated into the bulk increasing surface concentration of water and increasing the hydrogen bonding at this surface.[5] Recently, it has been shown that organic ions, including *p*-$NP^-$ can be found at air/aqueous interface.[6-8] Characterization of *p*-$NP^-$ at neat air/aqueous interfaces has been explored, determining not only the presence of the anion at the interface but also the angle at which it is oriented at the surface about the surface normal.[7] It has been shown that the angle of orientation with respect to the surface normal of *p*-$NP^-$ at the neat air/aqueous interface is concentration dependent. As surface concentration of *p*-$NP^-$ increases the orientation angle increases with respect to the surface normal.[7] This concentration dependence of the surface orientation angle contrasts with the nature of *p*-NP orientation at the air/aqueous interface, as it has been shown to be invariant as concentration is varied.[7, 9] The differences present between *p*-NP and *p*-$NP^-$ may be due to the electron density differences of the two molecules. Figure 1.1 shows the structures of *p*-NP and *p*-$NP^-$ as well as, the symmetry of these molecules that will be discussed in Chapter 2. This discrepancy of *p*-$NP^-$ versus *p*-NP concentration dependence of air/aqueous orientation angle presents the opportunity to determine the source of the mutable

orientation angle of *p*-NP⁻ at the interfacial region and allows insight to the elementary forces that determine orientation at air/aqueous interfaces.

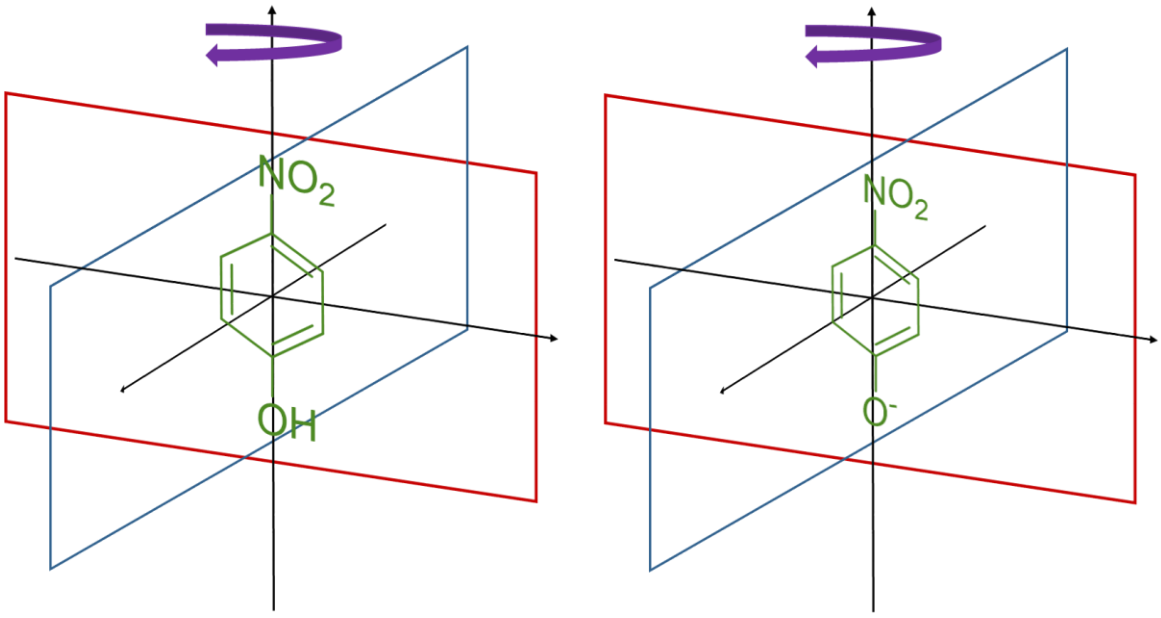


**Figure 1.1** Molecular Structure and symmetry operators of *p*-NP (left) and ($C_{2v}$ point group) *p*-NP⁻ (right)

Analysis of the orientation of *p*-NP⁻ at the air/aqueous interface is of primary importance in understanding interfacial chemistry. For example, modeling gas phase reactions, based on collision theory demonstrates the factors upon which a barrier to reaction may be present. This includes the orientation of the molecules upon collision.[10] Given, $k(T) = Z\rho \exp^{\left(\frac{E_a}{RT}\right)}$, is the mathematical form of the rate constant ($k$) at temperature ($T$) described by collision theory. Variables within this definition include steric factor ($\rho$), collision frequency ($Z$), activation energy ($E_a$), and the gas constant ($R$). Of interest regarding surface orientation is the definition of collision frequency; $Z = N_A \sigma_{AB} \sqrt{\frac{8k_B T}{\pi \mu_{AB}}}$. The collision frequency is dependent upon the reaction cross

section ($\sigma_{AB}$) which can be related to the orientation of the molecule. Because the air/aqueous interface present a change in environment from the polar aqueous phase to the non-polar air phase, the *p*-$NP^-$ is likely to have a unique alignment on the surface. Depicted in figure 1.2, this restriction of orientation could have effects on the reactivity of *p*-$NP^-$ adsorbed to the air/aqueous interface. Investigation of this reactivity is of core importance and has relevance to understanding photodegradation of *p*-$NP^-$ at such an interface.

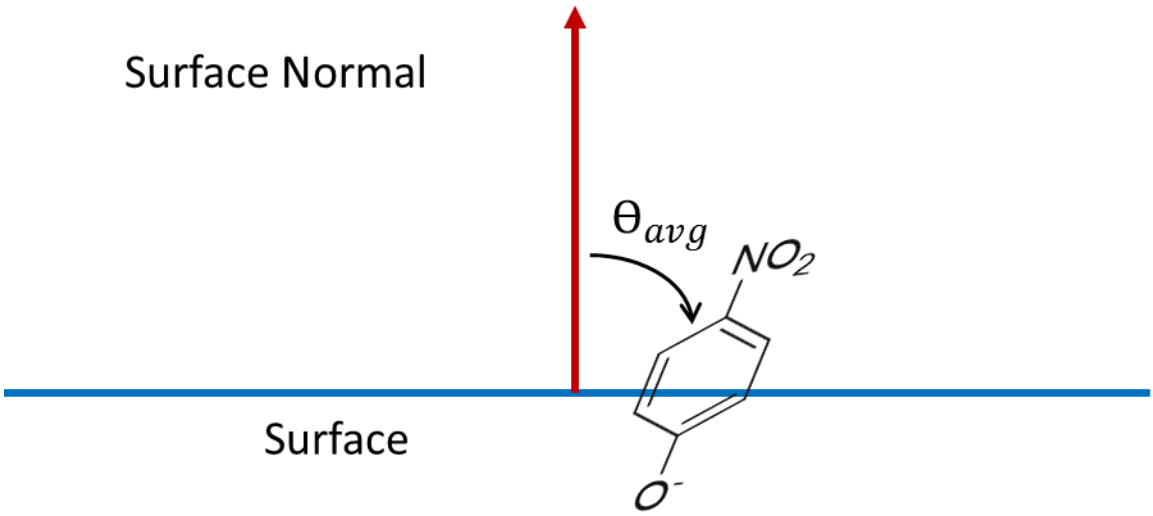


**Figure 1.2** Surface orientation of *p*-$NP^-$ with respect to the surface normal ( $\theta_{avg}$ )

The angle of orientation with respect to the surface normal can be measured using second harmonic generation (SHG). This is a spectrophotometric scattering phenomenon that is forbidden in centrosymmetric environments such as the bulk.[11-12] Centrosymmetric environments are those in which any point within the environment can be moved to the inverse of its position and the forces acting upon that point remain the same. Environments that are not centrosymmetric are known as anisotropic and are the only environments in which SHG is possible. SHG is a frequency doubling process, such that it occurs when two photons of one frequency interacts with anisotropic material and combine into a single photon of double the initial frequency.[11-12] Due to specific

selection rule, to be elaborated later, this interaction allows for surface bound species to be selectively investigated.[11-12] Due to the low probability of SHG occurrence the technique must be performed with a high intensity laser to increase incidents of this occurrence. This phenomenon can then be analyzed to give physical properties of *p*-$NP^-$ at the interfacial region of interest. Of importance, here within, is the air/aqueous interface.

## 1.2 Environmental Motivation

Human activity can drastically influence the environment unlike no other animal in nature. As mankind began to move from nomadic tribes to settled societies we began to change the environment more and more drastically.[13] Farming, animal husbandry, lumber, and human waste accumulation impacted the environment in various ways.[13-14] Recently, humans have greatly increased their ability to affect the environment drastically through the industrial revolution.[15] Industrialization has come with many benefits and many costs. The environmental costs of industrial production have been palpable since the beginnings of large scale production. Although the chemistry of such pollution was not understood, intuitively the harm to the environment was apparent. Charles Dickens prominently distilled images of this pollution and its change of the appearance of the world.[16] One benefit of such a revolution has been higher standards of living which allow us to switch our focus from merely surviving to many other goals, one of which should be the protection of our environment.[15] Through time our stewardship of the environment has increased with our technological successes, yet there remain waste materials that continue to contaminate the ecosystem. This problem is continual and dynamic, requiring weighing of costs and benefits. Scientific knowledge could allow for the costs to be reduced and would be a boon to our conservation of the Earth's various ecosystems as well as of health benefits to people exposed to such pollutants.

One such contaminant is *p*-NP qualified as priority pollutant by the EPA.[17] This organic molecule is water soluble allowing it to contaminate both soils and water sources. Generated by oil weathering and used in the production of parathion and acetaminophen, *p*-NP is integral to industrialized life. Industries using *p*-NP or generating *p*-NP as waste include pharmaceuticals, petrochemicals, pesticides, and plastics.[18-19] In addition, from these industrial sources, *p*-NP has been shown to be a photodegradation product of the herbicide nitrofen (2,4-Dichloro-1-(4-nitrophenoxy) benzene).[20-21] Because of the presence of *p*-NP within our modern industrial lifestyle it is necessary that it be studied and remediated in the environment.

Toxicity of *p*-NP has been studied and health risks to humans have been determined making *p*-NP investigation significant. Studies have been conducted on rats investigating health effects based on several routes of admission.[22] Depending upon the route of admission *p*-NP exposure resulted in effects on rats, lung size, enlarging liver, kidney blockage, and eye damage.[22] Being mammals, rats as an experimental corollary to humans are vital to determine related health effects of *p*-NP to humans. The safety data sheet (SDS) for *p*-NP states health effects from *p*-NP exposure and chronic exposure results in organ and nervous system toxicity.[23] Investigation provides evidence that nitrophenols can stimulate respiration of living cells and inhibit other energy functions of cells.[24] It has also been revealed *p*-NP can suppress metabolism of pyruvate in fish and rabbit testes.[24] Due to *p*-NP's use and contamination of the environment it is critical the chemistry regarding *p*-NP is well understood.

Aquatic environments, where *p*-NP may exist in the bulk phases (gas, liquid, solid) or at an interface, which is the region between two bulk phases. A ubiquitous interface within the environment in the form of oceans, lakes, and rivers is the air/aqueous interface constituting seventy-one percent of the Earth's surface.[25] In addition to the air/aqueous interface presented by

Earth's surface water, aerosols also present such an interface. Aerosols are a particularly important air/aqueous interface as they are found within the troposphere and influence the Earth's climate acting as a source for cloud nucleation.[26-27] It has also been shown that aerosols can be enriched in organic molecules and salts that could take molecules such as *p*-NP into the atmosphere.[26-27] Interfacial environments are distinguishable from bulk environments in the forces present.[11, 28] At these interfaces the forces lack a center of symmetry. In the case of the air/aqueous interface, the air can be thought of as a non-polar environment while the aqueous environment is polar in nature.[11, 28] Due to this unique environment, the chemistry at the interface may be unique compared to that of bulk chemistry.

Due to *p*-NP presence in the environment, coupled with its toxicity to humans and mammals, *p*-NP is an important molecule of study. Chemical knowledge of such a molecule provides practical application in waste remediation. Removal of *p*-NP from the environment has inherent benefits and if costs are managed through increased data it may be possible to eliminate risk to human populations.

## 1.3 Outline of Experimental Tools and Systems

Interest in surface chemistry requires tools and techniques that can selectively probe the interfacial region. Techniques that have been used to investigate the surface chemistry of plethora of systems have included atomic force microscopy (AFM), transmission electron microscopy (TEM), sum frequency generation (SFG), infrared spectroscopy (IR spectroscopy), and mass spectrometry (MS).[28-31] There are inherent benefits and costs when choosing an experimental tool. The system of interest is highly important and because the focus of this study involves liquid interfaces it was prudent to choose SHG as the experimental tool for probing *p*-$NP^-$ at various interfaces. Complementary to SHG is the use of the surface tensiometer which measures the

surface tension of a solvent to gain insight into the number density of solute molecules at the solvent/air interface.

Within this study, we probed *p*-$NP^-$ at different interfacial environments to elucidate their effect upon the orientation angle at the interface as well as determine the adsorption constant of *p*-$NP^-$ at these varied environments. The strategy proposed was to produce environments that would restrict the change of orientation angle with respect to the surface normal as well as chemical environments that can shift the change of this angle to different concentrations of *p*-$NP^-$ compared to the earlier concentration dependent studies.

We have studied multiple variations of the air/aqueous interface. Initially the use of hexane applied as a monolayer to the surface of *p*-$NP^-$ aqueous solution was attempted. Hexane would present a non-polar environment mimicking that of the air as well as possibly restrict the movement of *p*-$NP^-$ at the surface. The hexane/aqueous interface has been investigated previously with solutions of *p*-NP, the neutral molecule.[9, 32] Previous studies explored only one concentration of neutral *p*-NP at the hexane/aqueous interface and the surface orientation of *p*-NP was found to be approximately 45° with respect to the surface normal.[9, 32] Unfortunately, within our experimental setup hexane was an untenable solvent resulting in varied signal intensity making it impossible to do data analysis.

The first successful environmental variation was the addition of dipalmitoyl phosphatidylcholine (DPPC) lipid monolayer to the surface of *p*-$NP^-$ aqueous solutions. This lipid has a zwitterionic head group allowing solvation into aqueous solution while still being charge neutral in total. Within our experimental setup the quaternary-amine of choline maintains the charge on the head group inhibiting variation of charge with solution pH. DPPC was proposed to be introduced as a monolayer to the air/aqueous interface of *p*-$NP^-$ solutions to provide a structural

backbone to restrict the movement of *p*-$NP^-$ and limit variation of orientation angle as surface concentration of *p*-$NP^-$ increases. DPPC had previously been examined spectroscopically. The physical characteristics of a monolayer of DPPC is known, including the angle at which the lipid tails were oriented about the surface normal.[33] The major question we aimed to answer is to determine if the solvated head group with tails protruding into the air can restrict orientation angle change in adsorbed *p*-$NP^-$ with increasing *p*-$NP^-$ surface coverage.

The second environment that was investigated was electrolyte enriched environments of *p*-$NP^-$. Salts have been shown to affect the solvation of *p*-NP and other organic molecules.[22-23] Depending upon the salt that is utilized solvation of *p*-NP can increase, leading to lower surface excess, or solvation of *p*-NP can decrease, leading to higher surface excess of the *p*-NP molecule.[23-24] In addition, different salts have different surface activity, or propensity to be found at the air/aqueous interface and could have different effects on the orientation angle of *p*-$NP^-$.[25] Utilization of electrolytes to salt *p*-$NP^-$ out of solution increasing the surface excess resulting in higher concentrations of *p*-$NP^-$ at the surface than non-electrolytic *p*-$NP^-$ of comparable solution concentration was proposed to determine its effect upon orientation angle. The salts, sodium bromide (NaBr) and sodium chloride (NaCl) were investigated to understand a *p*-$NP^-$ interface that should be enriched in *p*-$NP^-$ compared to a non-electrolyte solution. Thereby we probed the influence of these salts on orientation angle of *p*-$NP^-$ and its variation, if any, as a function of its surface coverage.

In addition to the equilibrium studies, ultraviolet (UV) degradation of *p*-$NP^-$ at the air/aqueous interface was also investigated. It has previously been shown that *p*-$NP^-$ degradation on this interface occurred more slowly than reactions occurring in the bulk. To overcome such slow reaction times hydrogen peroxide ($H_2O_2$) was utilized to form hydroxyl radicals that would in turn

speed the reaction rates to time intervals upon which investigation can be performed. The rate of SHG change corresponding to *p*-$NP^-$ population decrease at the air/aqueous interface and can be plotted as a function of UV exposure to determine the rate of degradation.

Characterization of *p*-$NP^-$ at these various interfaces will allow elucidation of the forces present at the air/aqueous interface. This interface presents a unique and dynamic environment that has incomparable chemistry than that found within the bulk solution. Discussion herein will be focused on determining orientation, adsorption energy, and reactivity where possible within these diverse interfaces. This shall accomplish practical knowledge about the experimental system to be applied to environmental systems as well as the fundamental objective of accumulation of scientific knowledge.

## Chapter 2 - Experimental Techniques

Newton first showed that what we see as white light is composed of a spectrum. This spectrum of light is the result of varying wavelengths of the electromagnetic radiation. This fact is not only interesting but can be utilized for further understanding of the nature of reality. Later it was found that each element has a unique spectral series and understanding the formation of these series allowed for the introduction of quantized energy levels allowing for deeper level understanding of the world at the atomic level. Spectroscopy is the study of interaction of matter with electromagnetic radiation typically, the absorption, emission, and scattering of electromagnetic waves. A plethora of spectroscopic methods exist for investigating chemical systems. These include UV-visible spectroscopy, which utilizes electronic transitions, rotational and vibrational spectroscopies which utilize the motion of chemical bonds, and scattering spectroscopies such as Raman and Rayleigh scattering. These all offer unique ways to probe molecules and can give different insights into chemical behavior.

Achievements of the scientists of throughout history have led to such things as spectroscopy's utilization to characterize hosts of different environments. Application of infra-red spectroscopy for analysis of hydrocarbon mixtures, X-ray spectroscopy for investigating metal alloys and use on the Mars rover as well as the use of spectroscopy for analysis of distant stars and astronomical phenomenon have all expanded the horizon of knowledge. Given the power of such a tool for elucidating complex systems, spectroscopy is indeed equipped for exploring organic molecules at the air/aqueous interface.

## 2.1 Introduction to Second Harmonic Generation

The spectroscopic technique used in this investigation was SHG - a non-linear optical phenomenon. SHG is a second order non-linear process that can be described from a Taylor expansion of the induced polarization of a molecule (Equation 2.1).[11, 34-38]

$$P = \varepsilon_0 \left( \chi^{(1)} E + \chi^{(2)} EE + \chi^{(3)} EEE + ... \right) \qquad \textbf{Equation 2.1}$$

Induced polarization defined as dipole moment per unit volume, describes the interaction of electromagnetic waves with matter.[37, 39] The mathematical definition of this induced polarization is shown in equation 2.1 where *P* is the induced polarization, the dielectric is $\varepsilon_0$, susceptibility is denoted as $\chi$ within the Taylor expansion each ordered 1st, 2nd, 3rd, and so on. Within equation 2.1, *E* is the incident electromagnetic field. The second order SHG contribution to the overall induced polarization is $\chi^{(2)} EE$ in equation 2.1.

Within the applied electromagnetic field, molecules develop an induced dipole moment and these dipoles will align within the applied field as seen in figure 2.1. This induced polarization will happen within an environment that has a dielectric value that is accounted for within equation 2.1 which describes the resistance of that environment to the electric field. The susceptibility of the target molecule describes how easily, or susceptible, the molecule is to polarization by an electric field.[37-39] The combination of all these terms within equation 2.1 gives a physical description of the way in which electron clouds interact and line up within applied electric fields shown below in figure 2.1. As the terms within equation 2.1 become higher in order their overall contribution to

the induced polarization becomes greatly reduced. As such, it is evident that higher order processes are more likely with higher intensity.

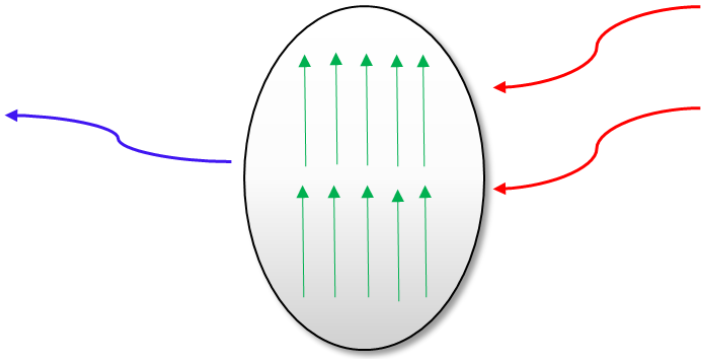

**Figure 2.1** Induced dipoles in an electric field – Two red waves denote incoming electric field of frequency corresponding to the visible color red. Blue wave denotes a single photon double the frequncy released from the interaction of two photons of frequency corresponding to red color. Arrows denote the alignment of the dipole moments of molecules (ex. *p*-$NP^{-}$) when interacting with electric field.

SHG is restricted to anisotropic medium and this is evident by exploring the second order terms within equation 2.1.[37] Anisotropy is a case in which there is no center of symmetry and so SHG should be forbidden in cases where a center of symmetry is present. Within equation 2.1 it can be seen if inverted the induced polarization will be $-P$. For this to hold true, the right hand term $\left(\chi^{(1)}E+\chi^{(2)}EE+\chi^{(3)}EEE+...\right)$, must also be negative after inversion.[37] The second order term, within this Taylor series would need to be negative, however because the incident field is squared

(*EE*) it would remain positive after inversion. This is true for any even ordered terms with in the formalism of induced polarization. For the induced polarizability to be inverted it necessitates the second order susceptibility to reduce to zero in media that have center of symmetry.[37] This fact allows for SHG to be surface selective because second order susceptibility is non-zero only in anisotropic media such as surfaces.

## 2.2 Hyperpolarizability and Resonance

The induced polarization acts as the source term for the field that results from the interaction of the incident field and the matter. Thus, the field generated from the 2nd order polarization leads to a field that can oscillate at a frequency that is the sum of the frequencies of the incident field.[11, 37, 40] In the case, where the two fields have the same frequency, the resulting field oscillates at twice the incident frequency. This is known as second harmonic generation. Equation 2.2 shows the SHG electric field is porportional to the second order susceptibility and that this second order suscesptibility can be described proprtionally to its number density ($N_S$), and the second order hyper-polarizability ( $\beta^{(2)}$), as shown below.[11, 35, 41]

$$E_{SHG} \propto \chi^{(2)} \propto N_s \left\langle \beta^{(2)} \right\rangle_{Orientation} \qquad \textbf{Equation 2.2}$$

The $\chi^{(2)}$ describes susceptibility of polarization at a macroscopic state. Shown in equation 2.2 the hyperpolarizability informs molecular scale polarization.[41] As a molecular tensor, the hyperpolarizability, $\beta^{(2)}$, allows for deduction of molecular orientation. This arises because the movement of the electron cloud is not uniform throughout the molecule and the magnitude of the hyperpolarizability of the molecule can be different within different coordinates of electromagnetic

interaction. Hyperpolarizability can be defined mathematically as a quantum event depicted in equation 2.3.[37, 40]

$$\beta_{ijk}^{(2)}\left(2\omega;\omega,\omega\right)=\sum_{g,e}\frac{\left\langle g\left|\vec{\mu}_j\right|v\right\rangle\left\langle v\left|\vec{\mu}_k\right|e\right\rangle\left\langle e\left|\vec{\mu}_i\right|g\right\rangle}{\left(\omega-\omega_{gv}+i\Gamma_{gv}\right)\left(2\omega-\omega_{eg}+i\Gamma_{eg}\right)} \qquad \textbf{Equation 2.3}$$

Equation 2.3 defines the hyperpolarizability, $\beta_{ijk}^{(2)}$ , as a sum of states with the bra-kets defining the probability of transitions between states.[37, 40] Dipole moments associated with the fundamental frequency of the incident photon, $\vec{\mu}_j$ and $\vec{\mu}_k$ , and the dipole associated with the SHG frequency, is $\vec{\mu}_i$. Molecular transitions are depicted in the denominator with $\omega_{gv}$ and $\omega_{eg}$ the frequencies associated with the transitions near the fundamental and second harmonic frequencies, respectively. These transitions between the ground, virtual, and excited state (*g, v, e)* can be seen in figure 2.2. Arising from the uncertainty in energy, lifetime broadening terms, $i\Gamma_{gv}$ and $i\Gamma_{eg}$ are included in the denominator corresponding to spectral broadening.

The second harmonic electric field generated from incident electromagnetic radiation at the anisotropic environment of interfaces involves the scattering of two photons.[37] Within this quantum process two photons of frequency $\omega$ are destroyed and a photon of frequency $2\omega$ is created. The two photon interaction transits through transient states also known as virtual states. The first photon excites the interacting molecule to a virtual state and upon incident of the second photon excites the molecule to a second virtual state and return to the ground state occurs when the photon $2\omega$ is created as seen in figure 2.2.[35-37, 40, 42] These virtual states are not eigenlevels of the free molecule but represent combined energy of a photons energy and the energy of an eigenstate of the molecule.[37] The probability of the process is very low and the intensity of the resulting SHG is low. If the molecule interacting with photons at an anisotropic media has an

electronic transition that closely overlaps the second virtual state, the SHG intensity can be enhanced. This overlap of virtual and electronic transition is known as a resonant enhancement. This facilitates probing solutions of much lower concentration or surface activity than is possible in its absence.[9, 40] Defined in equation 2.3 as the overlap between the frequencies of these transitions and the second harmonic or fundamental photon frequency the denominator approaches zero and the hyperpolarizability increases making SHG occurrence much more probable. Within this study the first electronic transition of *p*-$NP^-$ is roughly found at 400 nm making it expedient to use an incident wavelength of 800 nm.

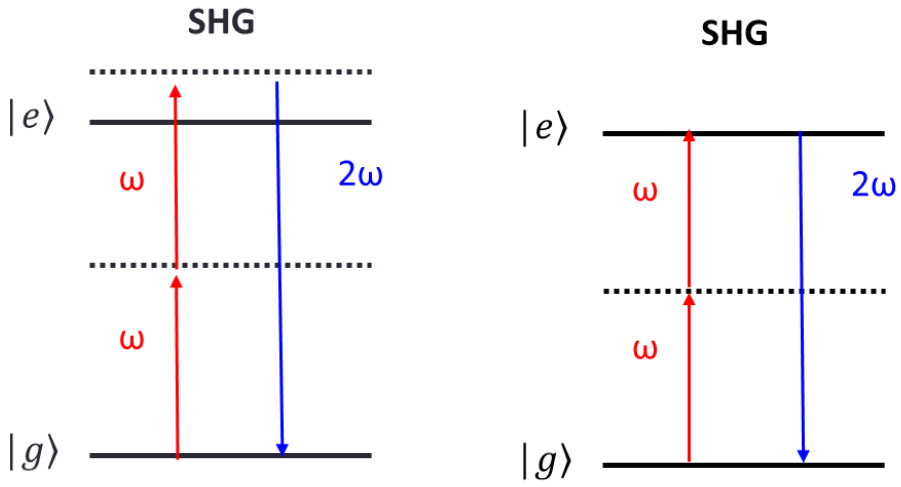


**Figure 2.2** Second Harmonic Transition (**left**- non-resonant SHG transition, **right**-resonant SHG Transition)

## 2.3 Laser and Experimental Setup

For this SHG experiment, a solid state Nd:YVO4 laser (Spectra-Physics, Millenia PRO 15sJ) which pumped a Ti:Sapphire Tsunami Oscillator (Spectra-Physics, 3941X1BB) to generate 70 fs pulses at 80 MHz has been used.

Tuning of the Tsunami Oscillator was done to produce a fundamental beam of 800 nm, which was directed toward the sample to be investigated, using various optical components, shown in figure 2.3. To prevent thermal effects from the fundamental beam, the laser beam was passed through a neutral density filter to diminish power before its incidence on the sample. The typical power at the sample was ca. 550 mW. Additionally, the sample dish was placed onto a translation stage that gently translated to prevent sample burning from the beam. Red filter was placed in the fundamental beam's path before introduction unto the sample to prevent all wavelenghts of light to impact the sample except that within the wavelengths corresponding to red light. Polarizer and a half-wave plate were used to select and manipulate the linear polarization of the light. The polarizers and half-wave plate were mounted to laser table and alligned with respect to the sample's surface normal such that p-polarized light (0°) is parallel to the surface normal and s-polarized light (90°) is perpendicular. Applying a lens, the fundamental beam was focused upon the sample surface maintaining a constant incident angle of 70°, necessary for establishing Fresnel coefficients discussed in section 2.4. The reflected second harmonic field was then passed through a blue filter to eliminate all wavelengths of light not corresponding to SHG. Again the beam is passed through a polarizer, upon which two distinct exit polarizations are investigated. After passing through the polarizer, the SHG signal is again focusesd using a lens before entering the monochromator.

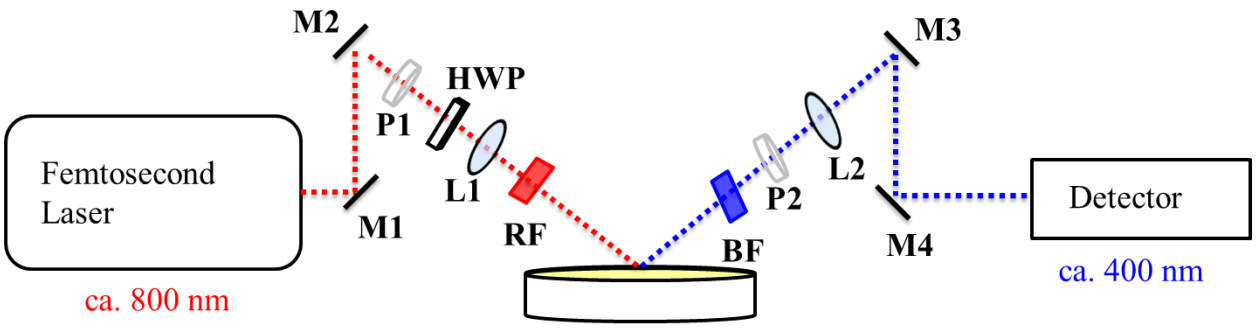


**Figure 2.3** Laser table layout (M=mirror, P=Polarizer, HWP= Half-wave plate, RF=red filter, BF=blue filter)

The monochromator (Acton SP2500, Princeton Instruments), uses gratings to select for particular wavelengths of light, of which we are concerned with those wavelengths denoting SHG (ca. 400 nm). After selection of narrow band of wavelengths consistent with SHG these photons are detected using a photomultiplier tube (PMT) (H11461P-01, Hamamatsu). Photocurrent generated from the PMT was led to a 350 MHz preamplifier (SR445A, Stanford Research Systems, Inc.) with three 50 Ω channels cascaded for a gain of 125x. This amplified signal flowed next into a single photon counter (SR400, Stanford Research Systems, Inc.) to be processed by LabView Software. Optical components (i.e. lenses and polarizers) and laser table equipment (i.e. translation stage) were purchased from ThorLabs and Newport corporation.

This thesis aims to detail *p*-$NP^{-}$ at various air/aqueous interfaces. Because the environments of samples are varied between different experiments discussion of the sample preparation will be discussed in each relevant chapter. Also, the prepartion of glassware and sample dishes will be presented with each discussion of the sepearate sample preparations.

## 2.4 Polarization Dependent Experiments and Molecular Orientation

To determine molecular orientation, SHG intensity has been measured as a function of input polarization. Polarization of light describes the direction in which ossicliation of the electromagnetic wave occurs. Before its incidence upon a sample surface the photons of fundamental frequency, ω, passes through a half-wave plate. Half-wave plates allow the selection of linearly polarized light as the fundamental beam tansits toward the sample surface. Input polarization can be varied and differences in the intensity of resulting SHG can be collected for selection of only certain polarizations of light. In our experiment, the input polarization can be varied from 0° to 360°. The polarization data is collected in two disparate exit polarizations allowing for molecular orientation calculation. The two exit polarizations collected are P-Out, which is parallel to the sample surface normal, and S-out which is perpendicular to this surface normal. Figure 2.4 shows a representation of sample surface with incoming and exiting light of the polarizations disscussed.

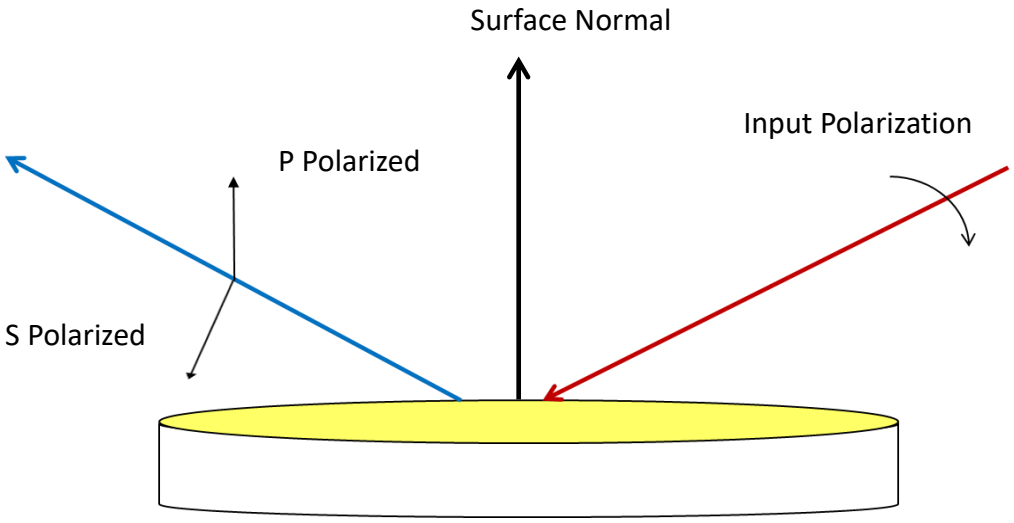


**Figure 2.4** Input and Exit Polarization – Input polarization is varied over 360° with two fixed exit polarizations - S-Polarization - 90°; P-Polarization-0°

Anisotropy data collected can then be analyzed and component susceptibility values can be solved for by fitting, assuming the molecule of interest is of the $C_{2V}$ symmetry point group, which is true for *p*-$NP^-$.[35, 42] The way in which *p*-$NP^-$ and *p*-NP can be characterized within the symmetry operators defining the $C_{2V}$ point group is shown in figure 1.1. The $C_{2V}$ point group is unaxial in symmetry and contains two mirror planes. Molecules of this point group have identical symmetry operators and interact with electromagnetic fields in identical ways. Due to this symmetry there are susceptibility terms that vanish simplifying the analysis and making *p*-$NP^-$ an ideal target molecule.[37] This is because the frame upon which we view the sample, the lab frame, is different from the frame upon which the molecule is oriented, the molecular frame. It is therefore possible for to pivot frames to make absolute observations about the molecule of interest. This rotation between frames is done by utilization of Euler angles through rotation matrices moving the vectors from the molecular frame to the lab frame.[43] Found in equation 2.4 the second order susceptibility, which is a macroscopic property and is measured in the lab frame with a coordinate system of *I*, *J*, and *K* that is a sum of the transformation of the molecular frame hyperpolarizabilities in the *i', j'*, and *k'* coordinate system.[35, 42] In equation 2.4, the $R_{\lambda\lambda'}$ represents elements of the Euler coordinate transformation from the molecular frame to the lab frame.

$$\chi_{IJK}^{(2)} = N_s \sum_{i'j'k'=x'y'z'} \left\langle R_{Ii'} R_{Jj'} R_{Kk'} \right\rangle \beta_{i'j'k'}^{(2)} \qquad \textbf{Equation 2.4}$$

Equation 2.5 featured below is used to fit the S-Out polarization anisotropy data. Within this equation, *a*, is a Fresnel coeffecient that describes the amount of energy transmitted through the medium that is solved for using Maxwell's equations for electromagnetism.[32, 38] The interface is thought to be an average between the two media; for example, the average of the refractive indices of air and water. This is the assumption used to describe the amount of energy transferred into the

medium upon which the interaction of photon and *p*-$NP^-$ occurs. Within equation 2.5 and equation 2.6 the input polarization angle of the incident electromagnetic field is defined as γ. Fitting the data to this curve allows for the solution of, $\chi_{ijk}$ , with, *i*, being the coordinate of the SHG field, *j*, is the coordinate of the first fundamental field photon and, *k*, is the coordinate of the second fundamental field photon. The $\chi_{XXZ}$ solved for within the S-Out curve fitting is then used as a parameter to fit the P-Out anisotropy data because it is also found in equation 2.6 and limits error when solving for the remaining susceptibilities. Equation 2.6 is used to fit the P-out anisotropy data and the remaining component susceptibilities can be found.

$$I_{2\omega,s} \propto \left| a_1 \chi^{(2)}_{XXZ} \sin(2\gamma) \right|^2 \qquad \textbf{Equation 2.5}$$

$$I_{2\omega,p} \propto \left| \left( a_2 \chi^{(2)}_{XXZ} + a_3 \chi^{(2)}_{ZXX} + a_4 \chi^{(2)}_{ZZZ} \right) \cos^2(\gamma) + a_5 \chi^{(2)}_{ZXX} \sin^2(\gamma) \right|^2 \qquad \textbf{Equation 2.6}$$

The component susceptibilities solved for using equation 2.5 and equation 2.6 have physical interpretations in the orientation of the angle of the molecule of interest at the surface with respect to the surface normal.[34, 42] Because component hyperpolarizabilities are not equal within each coordinate system the ratios of these macroscopic susceptibilites can be used to elucidate the orientation about the surface normal. Equation 2.7 is applied to deduce the average angle of orientation with respect to the surface normal. This angle is described by the ratio of the seperate susceptibilities solved for in equation 2.5 and equation 2.6.[35]

$$\theta_{avg} = \cos^{-1}\left( \sqrt{\frac{\chi_{ZZZ} - \chi_{ZXX} + \chi_{XXZ}}{\chi_{ZZZ} + 3\chi_{XXZ} - \chi_{ZXX}}} \right) \qquad \textbf{Equation 2.7}$$

By solving for $\theta$ over a range of concentrations we can find how the average orientation angle changes with respect to surface excess. This surface excess is related to the bulk

concentration. Although number density is a component of the second order susceptiblity, we note that SHG also depends on the molecular orientation. Therefore, it is not trivial to obtain relative number density of adsorbed species.

## 2.5 Surface Excess and Adsoroption Isotherm

SHG is not able to arrive at surface excess information in the case of planar surfaces. Surface tensiometer is able to probe the change in surface tension of a solution and has been used in our group to identify surface excess of the solute of interest. Coupled with the Gibbs adsorption equation the surface activity can be solved. The environment described in equation 2.8 is that of two systems, $\alpha$ and $\beta$ that form an interface.[44] The number of total moles of solute *i* within these two systems is defined as $n_i$. $C_i^{\alpha,\beta}$ defines the concentration of solute *i* in each environment and $V_{\alpha,\beta}$ defines the volume of these two systems. These terms are all used to derive $n_i^{\sigma}$ which defines the moles of solute, *i*, found in the interfacial region.

$$n_i^{\sigma} = n_i - \left(C_i^{\alpha} V_{\alpha} + C_i^{\beta} V_{\beta}\right) \qquad \textbf{Equation 2.8}$$

Equation 2.8 describes the number of moles found within the dividing surface. This interface is a two-dimensional plane and treating it as such the concentration of the interfacial solute can be described by equation 2.9.[44] This concentration, $\Gamma_i^{(\alpha)}$, is described with repsect to area of the Gibbs dividing surface, $A^{\sigma}$.

$$\Gamma_i^{(\alpha)} = \frac{n_i^{\sigma}}{A^{\sigma}} \qquad \textbf{Equation 2.9}$$

Building upon the definitions of equation 2.8 and equation 2.9 the surface tension of the solution, $\sigma$, can be described as a function of adsorption of solute molecules to the dividing

surface. The surface excess can be described using equation 2.10.[44] The surface excess, $\Gamma$, is defined as the change in surface tension, $\sigma$, with respect to the change in concentrtion, *c*. The key idea is that surface population can be obtained via the measurement of surface tension. In general, the experimental change in surface tension with increasing concentration of solute, *c*, can be described by an empirical fit function. The simulated data is then used to calculate the derivative; i.e., the rate of change of surface tension with respect to solute concentration. Once this is known then surface excess can be calucated using equation 2.10.

$$\Gamma = -\frac{1}{RT}\frac{d\sigma}{d\ln c} \qquad \textbf{Equation 2.10}$$

The plot of surface excess as a fuction of equilibrium concentration is known as an adsorption isotherm. This adsorption isotherm makes possible the solving for the equilibrium constant of adsorption ($K_{ads}$) of a species to the interfacial regionIsotherms plot the concentration of the molecule of interest at the interfacial region as a function of bulk concentration to determine its propensity for this interface. These data are conventionally fit with the Langmuir isotherm equation assuming no intermolecular interactions at the interfacial region. The Langmuir isotherm equation is defined in Equation 2.11 where $\theta_f$ is the fractional surface coverage, $N_s$, the number of surface adsorbed molecules, $N_{tot}$, is the effective surface sites, $C$, is the volumetric concentration of the adsorbate, and $K$ is the adsorption equilibrium constant.[45] Although SHG measurements cannot yield surface population information from a planar surface, it is however possible to determine the the adsorption equilibrium constant based on the change of $E_{SHG}$ with concentration. In such cases, Langmuir model is also applicable. This will be discussed further in chapter 4. Also, note that the *K* solved for in equation 2.11 can be used to find the free energy of

absorption of the solute at the interfacial region. The Gibbs free energy of adsorption is given by equation 2.12, where, R, is the gas constant at a constant temperature, *T*.

$$\theta_f = \frac{N_S}{N_{tot}} = \frac{KC}{1+KC} \quad \textbf{Equation 2.11}$$

$$\Delta G = -RT\ln(K_{ads}) \quad \textbf{Equation 2.12}$$

This concludes the basic understanding of the theoretical and experimental background of this project. Next we transition to the experimental results.

# Chapter 3 – Monolayer Restriction of *p*-nitrophenolate at Interface

It has been shown that the orientation angle of *p*-$NP^-$ changes with respect to the surface normal as its surface population increases.[7] The need arises to investigate the reason behind the change of this angle. One approach of elucidating the source of this change is to restrict the movement of *p*-$NP^-$ at the air/aqueous interface. The method by which we aimed to restrict *p*-$NP^-$ was by the introduction of a molecular monolayer to the air/aqueous interface with the intention of sterically hindering the angle change as surface excess is increased. The underlying hypothesis was that by providing a support the molecular interaction responsible for the orientation change can be elucidated.

## 3.1 Initial Endeavors Involving Liquid/Liquid Interface

The first attempt at restricting this change in orientation angle with respect to the surface normal was the use of a hexane layer. Hexane had been investigated as a liquid-liquid interface with *p*-NP solutions previously.[9, 32] Within such investigations it was shown that *p*-NP of a concentration of 0.05 M had a molecular orientation of 48° and 45° with respect to the surface normal between air/aqueous and hexane/aqueous environment, respectively.[9] The adsorption of *p*-NP to the hexane/aqueous interface was slightly different for the two interfaces. The energy of adsorption was found to be $-16.4\frac{kJ}{mol}$ and $-17.2\frac{kJ}{mol}$ for the air/aqueous and hexane/aqueous interfaces, respectively.[9] It had also been discovered previously that liquid hexane did not produce much of a second harmonic signal because it is centrosymmetric.[32] This allows for targeting of *p*-$NP^-$ at the hexane/aqueous interface.

The hexane/aqueous interface seemed promising for understanding oil/aqueous interface and its effect on *p*-$NP^-$. We began by probing air/liquid interfaces of pH 13 water and liquid

hexane, as well as the liquid/liquid interface of these two solvents to determine the SHG background. These experimental results are presented in figure 3.1(a). Hexane had little contribution to SHG signal and the opportunity for its use within this experiment was still possible. However, reproducibility of the SHG intensity from the hexane/aqueous interface was difficult to achieve with our experimental setup. Anisotropy data were collected for *p*-$NP^-$ at the hexane/aqueous interface and consistently the intensity would fluctuate during data collection. As an example, figure 3.1(b) shows representative anisotropy data and the fluctuation over the duration. Typically, anisotropy data should be symmetrical; that is, intensity profile from 0° to 180° polarization angle should be the same as from 180° to 360°. However, that was not the case and is indicative of a changing interfacial environment over the duration of data collection, which lasts approximately 15 minutes. Although, the experiments represented by figure 3.1(b) have reproducibility issues, SHG intensity is increased from the pH 13 hexane interface represented in figure 3.1(a) evidence that *p*-$NP^-$ is adsorbing to the hexane/aqueous interface. As it became clear that the initial setup was not possible, we probed this environment further to determine the source of the problem. Determination of the effect of different volumes of hexane introduced to *p*-$NP^-$ solutions was found not to ameliorate the issue of variance with time. The vapor pressure of hexane is relatively high, 153 mmHg at 25°C compared to the vapor pressure of water, 23.756 mmHg at 25°C.[46-47] This lends evidence to the hypothesis that hexane is evaporating and the interfacial region is changing during sample measurement making the data collection asymmetric and given our laboratory setup it was not feasible to continue with hexane as a viable experimental resource.

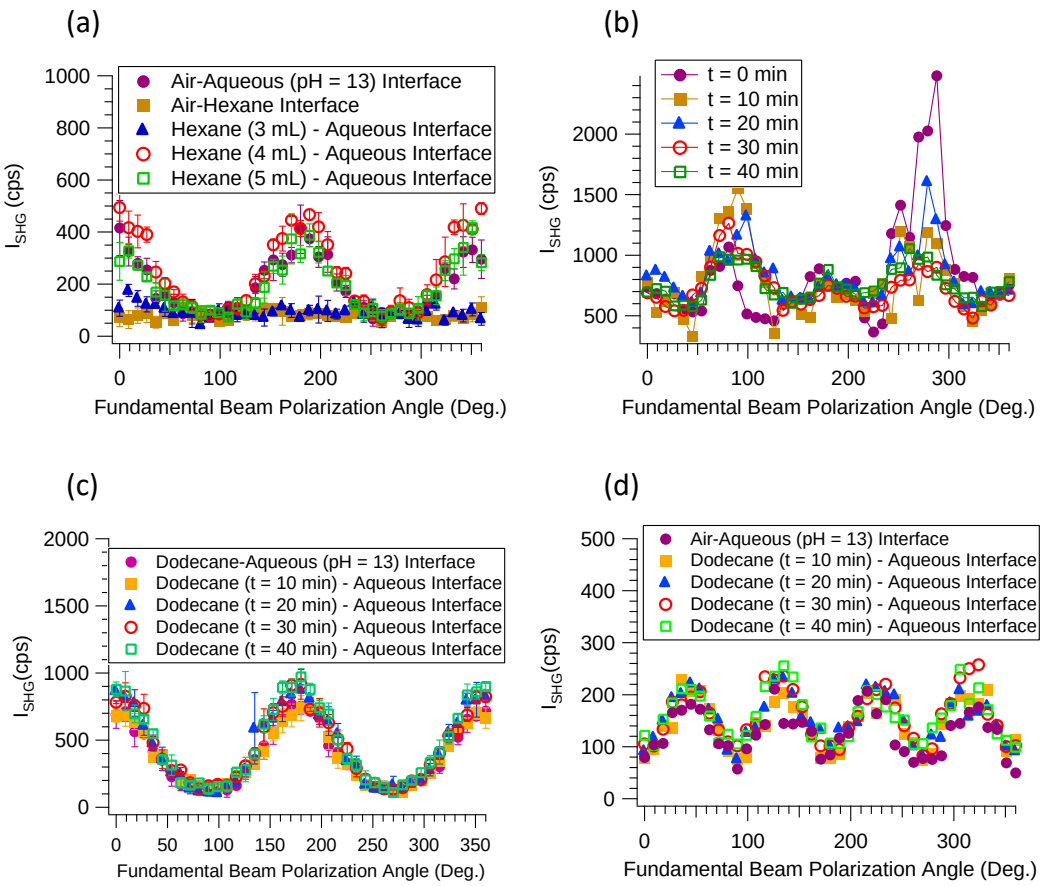


**Figure 3.1** Polarization anisotropy data of hexane and dodecane experiments- Within pH13 describes investigation of the solvent water at pH13 at air/aqueous interface (a) Varying thicknesses of hexane (p-out), (b) Hexane/aqueous layer over time evaporation of hexane can be seen to make this data highly variable, (c) Dodecane monitored over time (p-out), and (d) Dodecane monitored over time (s-out)

Dodecane having a vapor pressure of 47.74 mmHg at 126°C seemed to be a wise transition to determine if *p*-$NP^-$ molecular orientation could be restricted at the interfacial region.[48] Dodecane would still model a non-polar interface and being a long chain alkane it would allow for a structural backbone to enable *p*-$NP^-$ orientation restriction. However, dodecane proved to be difficult in a distinctly different way than hexane. Shown in figure 3.1 (c) and figure 3.1 (d) is anisotropy data

that demonstrates the difficulty of using dodecane as the structural backbone for *p*-$NP^-$ at the interfacial region. Dodecane shows significant SHG signal for both p-out and s-out polarizations. This SHG signal originating from dodecane would represent great difficulty in isolating contribution due to *p*-$NP^-$ alone. Due to this difficulty dodecane was quickly abandoned as viable option for our experimental purposes.

## 3.2 *p*-$NP^-$ at Air/Lipid/Aqueous Interface

Subsequently, we switched to probing *p*-$NP^-$ at the air/aqueous interface in the presence of a zwitterionic lipid molecule, DPPC. DPPC containing a zwitterionic head group was ideal because it allowed solvation of the lipid into the aqueous phase while having no overall charge so the surface charge remained unaffected allowing for elimination of possible extra variables in *p*-$NP^-$ adsorption to the interface. Referencing figure 3.2 it can be seen the head group of DPPC, phosphatidylcholine is composed of a quaternary amine that is positively charged and a negatively charged phosphate group. The pH of *p*-$NP^-$ solutions used for experiments are highly basic at pH 13, this ensures not only *p*-$NP^-$ exists as an anion but also DPPC will remain overall neutral and the zwitterionic head group will remain charged with a positive quaternary amine and negative phosphate group. The tail groups of DPPC are palmitic acid, a sixteen-carbon saturated fatty acid. This long fatty acid chain is non-polar and could act as support to restrict *p*-$NP^-$ at the air/aqueous interface. Evaporation of DPPC would also not be an issue due to low vapor pressure of lipids evident in the vapor pressure of the constituent tail group palmitic acid being $3.8\times10^{-7}$ mmHg at 25°C.[46]

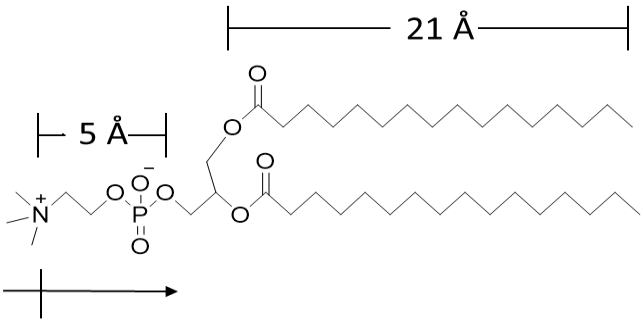


**Figure 3.2** DPPC Lipid dimensions and head group dipole

In addition to the physical properties of DPPC there was also literature with information about DPPC at air/liquid interfaces bolstering the proficiency of its use as a molecular support for *p*-$NP^-$ at the air/aqueous interface. Within literature regarding Langmuir Trough probing of a DPPC monolayer it has been shown DPPC occupies an area 50 $Å^2$ per molecule.[33] DPPC monolayer was probed using sum frequency generation and the fatty acid chains were found to have a tilt of 25° with respect to the surface normal.[33] The phosphatidylcholine head group is suggested to be solvated parallel to the monolayer surface.[49] Computational analysis suggests the angle between the P-N dipole of the head group and the water surface is 5° or roughly parallel.[50] The refractive index of DPPC was also found allowing for understanding of the way in which photons pass through the monolayer to interact with *p*-$NP^-$, this refractive index is $1.478 \pm 0.006$ for the experimental wavelength.[51] This all gives basis for the analysis of our experiments regarding effects of introduction of DPPC air/aqueous interface on *p*-$NP^-$ adsorption and orientation.

Within our experimental setup the sample containers were Teflon dishes with an area of ~ 30 $cm^2$. These sample containers were prepared by first soaking them in aqua regia for half an hour followed by 20 rinses of de-ionized water and 3 rinses of Millipore (Milli-Q, 18.2 MΩ·cm) water to ensure a pristinely clean surface. Samples of *p*-$NP^-$ were prepared using *p*-NP crystal (Reagent

Grade, ≥ 99%, 241326-50G), purchased from Sigma-Aldrich, dissolved into pH 13 Millipore water. Solutions were made basic with sodium hydroxide (ACS reagent, ≥97.0%, 221465-500G), purchased from Sigma-Aldrich. Concentrations of *p*-$NP^-$ solution were made from 5 mM to the saturation at 130 mM. DPPC was made using solid 1,2-Dipalmitoyl-sn-glycero-3-phosphocholine (Semisynthetic, ≥99.0%, 1002095071), purchased from Sigma-Aldrich, dissolved in chloroform at a concentration of 0.5 mg/mL made fresh before each trial and stored in a freezer. Before introduction to the surface, DPPC solution was allowed to reach room temperature and well mixed before injection and returned to the freezer between each sample of *p*-$NP^-$. Solutions of *p*-$NP^-$ were transferred to sample dishes at a volume of 50 mL and allowed to equilibrate before DPPC introduction. Upon injection of DPPC to the surface of solutions evaporation of chloroform was allowed for 15 minutes to ensure that the monolayer was purely DPPC.

First phase of the DPPC experiment 14 $\mu L$ of DPPC solution was introduced to the surface of *p*-$NP^-$ solutions at 5 different points to create a monolayer. This volume of DPPC would theoretically create a monolayer with roughly 50 $Å^2$ per molecule. The points of introduction of DPPC to the surface as well as dimensions of the sample dish can be seen in figure 3.3. During data collection for *p*-$NP^-$ solutions with 14 $\mu L$ of DPPC it was found the anisotropy data was not reproducible. Variability within data sets led us to believe there was either too much DPPC causing collapse of the monolayer or insufficient DPPC to form a monolayer. Concentrations of DPPC were held constant at 0.5 mg/mL and multiple volumes of DPPC were then examined to see if reproducibility of anisotropy data was improved. The volumes ranged from 10 $\mu L$ to 23 $\mu L$ with 20 $\mu L$ remedying the inconsistency within the data. The 20 $\mu L$ volume DPPC would result in a coverage with area per molecule roughly 36 $Å^2$. This discrepancy could be due to error within techniques adding the DPPC to the *p*-$NP^-$ surface. The limits of the accuracy of weighing out small

amount of sample and possible loss of material during transferring the sample may have played a role in this discrepancy. Nonetheless, to be consistent, for all the experiments, a volume of 20 $\mu L$ was dropped on the sample dish using a micro-syringe. The surface area of the dish calculated to determine the amount of DPPC to introduce to the sample assumes the area occupied by the lipid is a two-dimensional circle. If curvature of the solution was present at this surface it would change the volume needed to create the monolayer explaining the discrepancy between the theoretical volume of DPPC calculated and the experimental volume found to solve irregularities within anisotropy data collected.

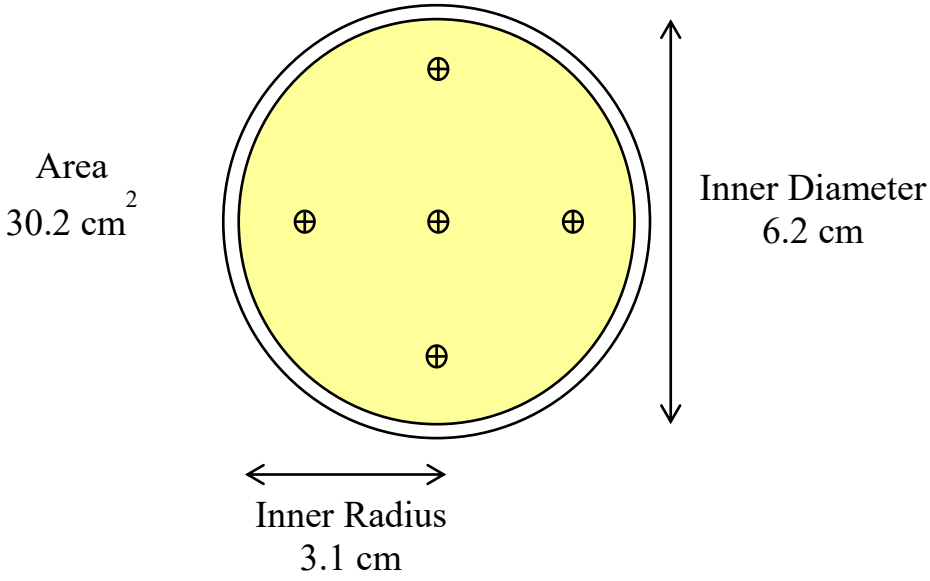


**Figure 3.3** Points of Introduction of DPPC to *p*-$NP^-$ samples and dimensions of sample dish

## 3.3 Orientation of *p*-$NP^-$ at the Air/DPPC/Aqueous Interface

Upon solving technical issues with the experimental setup of DPPC monolayer at the air/aqueous interface of *p*-$NP^-$ solutions quality anisotropy data were collected and analyzed. Analysis of anisotropy data was performed using fit equations 2.5 and 2.6. Within these equations

there are Fresnel coefficients that describe the degree to which an incoming electric field penetrates the interfacial layer denoted as $a_1$ through $a_5$ in equations 2.5 and 2.6. These were solved and can be found in table 3.1.

**Table 3.1** Fresnel Coefficients for fit equations with regards to DPPC/ *p*-$NP^-$ solution interface

| $a_1$ | $a_2$ | $a_3$ | $a_4$ | $a_5$ |
|---|---|---|---|---|
| 0.838286646 | -0.84779209 | 0.420935729 | 0.338724968 | 0.838316261 |

Utilizing the coefficients above, anisotropy data can be fit and component values of the second order susceptibility, $\chi^{(2)}$, can be solved allowing for analysis of the orientation of *p*-$NP^-$ at the interfacial region. Found in figure 3.4 are examples of DPPC anisotropy data and fit lines used to solve susceptibilities relevant to orientation analysis.

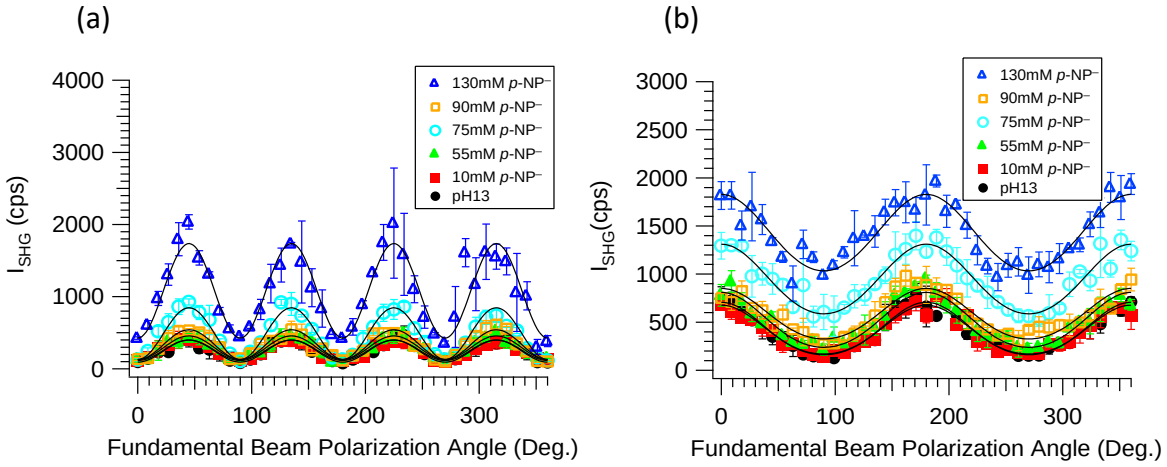


**Figure 3.4** (a) S-Out polarization data of selected concentrations of *p*-$NP^-$ at the air/aqueous interface with a DPPC monolayer, (b) P-Out polarization data of selected concentrations of *p*-$NP^-$ at the air/aqueous interface with a DPPC monolayer

Conventionally when analyzing anisotropy data, the control experiment is subtracted from the data to eliminate background SHG contribution. Orientation angle analyses based on these data were carried out both by subtracting the air/aqueous (pH 13) intensity and without subtraction. The data included in this thesis however only presents the data that does not include this pH 13 sample subtraction. In certain cases, when pH 13 intensity is subtracted, the orientation angle corresponding to the lower concentration *p*-$NP^-$ samples are not easily obtainable and/or show large uncertainties after propagation of error. This is because the values of the control and lower concentration *p*-$NP^-$ samples are comparable and thus, subtraction of pH 13 intensity removes the ability to fit low concentration data. To analyze dilute *p*-$NP^-$ it was necessary to proceed with analysis of raw data. Otherwise, the orientation angle for low surface coverage was not obtainable. It must be emphasized whether the pH 13 intensity was subtracted or not the trend in the orientation angle variation remained the same. This was certainly verified by comparing the two analysis methods for the case of electrolyte interfaces, which is presented in chapter 4. For consistency, herein we opted to present the orientation angle calculation based on the raw data analysis only.

As mentioned earlier, applying equation 2.7 to the susceptibility values determined from fitting of DPPC anisotropy data, average orientation of *p*-$NP^-$ at this interface can be elucidated.

In figure 3.5(a-d) representative plots of several experimental trials of *p*-$NP^-$ orientation at the air/aqueous interface with a monolayer of DPPC. Also, the average *p*-$NP^-$ orientation at the neat air/aqueous interface plotted with averaged *p*-$NP^-$ orientation at the air/aqueous interface with DPPC monolayer is shown in figure 3.5(d). The latter experimental data was collected previously in our group[7] and is presented here alongside the new findings to highlight the comparison. Through the concentration range used (5mM – 130mM *p*-$NP^-$) the difference between average orientation angles can be seen between *p*-$NP^-$ at the air/aqueous interface and *p*-$NP^-$ at this

interface with introduction of a DPPC monolayer. As concentration of *p*-NP$^-$ is increased the average orientation with respect to the surface normal remains unchanged maintaining an angle of about 30°. In contrast, the average orientation of *p*-NP$^-$ at the air/aqueous interface in the absence of a lipid monolayer, changes as a function of concentration.[7] Within the same concentration range *p*-NP$^-$ in a non-modified environment undergoes a widening angle change with respect to the surface normal, varying from ca. 35° to ca. 50°.[7]

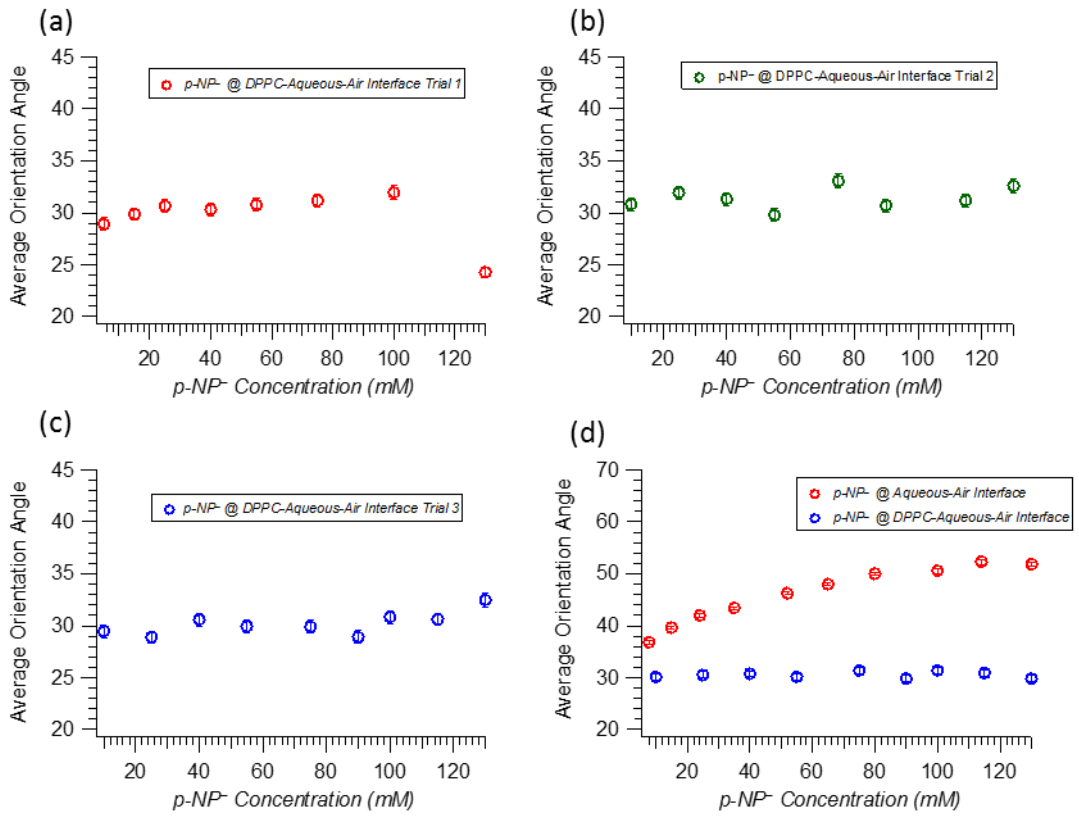


**Figure 3.5** (a) Average Orientation Angle of *p*-NP$^-$ at the air/aqueous interface with DPPC monolayer as a function of concentration (trial 1), (b) (trial 2), (c) (trial 3), (d) Average Orientation Angle of *p*-NP$^-$ as a function concentration with presence (blue) and absence (red) of DPPC monolayer[7]

The discrepancy of the plots of average orientation angle versus *p*-$NP^-$ concentration, between DPPC introduction and absence of this lipid monolayer supports the idea that DPPC can restrict the movement of *p*-$NP^-$ at the air/aqueous interface. Note, the literature describes the tilt of the chains of DPPC with respect to the surface normal as 25°.[33] Interestingly the average orientation angle of *p*-$NP^-$ at the air/aqueous interface with a DPPC monolayer is roughly 30° (close to 25°) versus the surface normal. Because of this apparent similarity in orientation angles, it can be surmised that *p*-$NP^-$ is penetrating the interface between these tail groups and this restricts the ability of *p*-$NP^-$ to change orientation as the surface population increases, a function of increased bulk concentration of *p*-$NP^-$ solutions. Although it cannot be proven via SHG analysis how *p*-$NP^-$ penetrates the interfacial region a depiction of possible configuration of *p*-$NP^-$ at this interface is shown in figure 3.6.

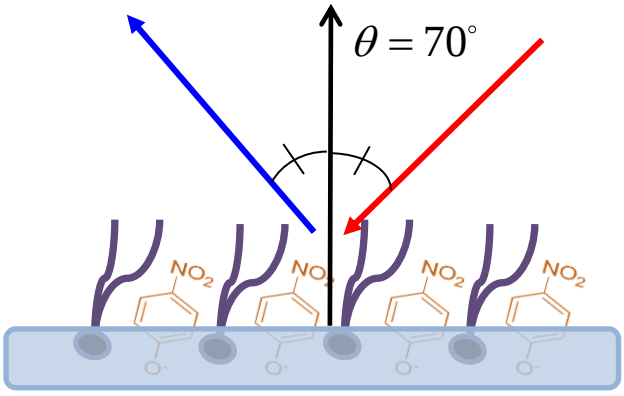


**Figure 3.6** Representation of orientation of *p*-$NP^-$ at the air/aqueous interface with DPPC monolayer

## 3.4 Adsorption Isotherm of p-$NP^-$ at the Air/DPPC/Aqueous Interface

Referring to equation 2.2, we note that $E_{SHG}$ field is directly proportional to the number density. In the case of *p*-$NP^-$, which is resonant, we can calculate the second harmonic field, $\left(E_{SHG}\right)$, from the raw SHG intensity as follows:

$$E_{SHG} = \sqrt{I_{SHG,raw}} - \sqrt{I_{SHG,solvent}}$$ **Equation 3.1**

In this equation, $I_{SHG,raw}$ and $I_{SHG,solvent}$ are SHG intensities from the *p*-NP$^-$ and the pH 13-DPPC interfaces, respectively. A plot of the $E_{SHG}$, average of 54° and 234° input polarizations, as a function of concentration is shown in figure 3.8. In this case, the SHG output polarization was set at 0° and the input polarization of 54° was used. This angle, which is the orientation insensitive angle, was calculated based on the Fresnel coefficients (Table 3.1) using the equation 3.2.[52]

$$\gamma^* = \cos^{-1}\left(\frac{a_5}{3a_4 + a_5 - a_2 - a_3}\right)^{\frac{1}{2}}$$ **Equation 3.2**

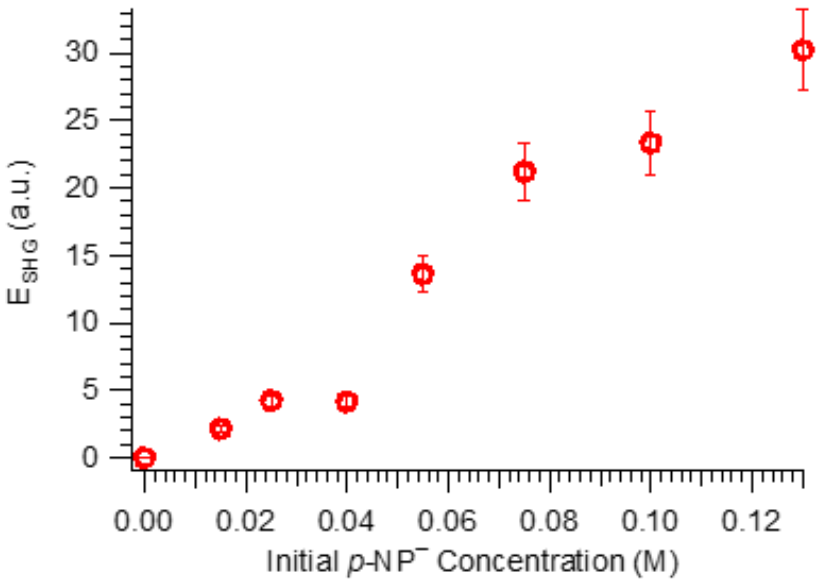


**Figure 3.7** Representative isotherm of *p*-NP$^-$ at the air/aqueous interface with a DPPC monolayer

Stated in Chapter 2, conventionally Langmuir approximation is used to fit isotherm data. With equation 2.11 it would be possible to retrieve the adsorption equilibrium constant from an isotherm such as the one represented in figure 3.7. After solving for the equilibrium constant equation 2.12 can be used to find the free energy of adsorption for *p*-$NP^-$ at the air/aqueous interface with DPPC monolayer. However, the adsorption figure shown in figure 3.7 suggest that *p*-$NP^-$ adsorption to the aqueous/DPPC interface does not obey the Langmuir mode. This is possibly because this approximation assumes there are no intermolecular interactions between adsorbed molecules and there exists no competition for surface sites. Because of the presence of DPPC as well as *p*-$NP^-$ at the air/aqueous interface, competition and/or interaction between these two adsorbed molecules may be present.

# Chapter 4 – Electrolyte Effects on *p*-nitrophenolate at Interface

Evidence thus far has shown the air/aqueous interface to be dynamic. Specifically, at the neat air/aqueous interface the orientation of *p*-$NP^-$ is subject to change with increased surface population, as well as be restricted in presence of a lipid monolayer. To find the source of this orientation angle change we ask the following questions. Is it possible to increase the surface population of *p*-$NP^-$ beyond that seen in saturated solution? Can counter-ion introduction stabilize the changing orientation, and therby keep *p*-$NP^-$ orientation unchanged as surface population increases? To answer such questions it was necessary to study *p*-$NP^-$ solutions with high ionic at the air/aqueous interface. However, at the same time it is important to understand the influence of the salt on the surface population of the *p*-$NP^-$.

## 4.1 Effects of High Ionic Strength Solutions

Salt effects are those effects that occur due to introduction of electrolytes to solutions. Highly soluble salts will preferentially dissolve into solution leaving less soluble molecules to salt-out.[41] In contrast, salting-in is the use of denaturants or salts with large ions to make molecules soluble.[53] Investigations of the effects of denaturants, such as urea, and electrolytes, such as lithium chloride on *p*-NP, a neutral molecule, have been carried out previously.[41, 53] These studies were performed with SHG to determine increases and decreases in SHG intensity to determine the effects of different molecules on *p*-NP adsorption at the air/aqueous interface. Within these inquiries it was found that lithium perchlorate, guanidinium hydrochloride, and urea were shown to decrease SHG intensity denoting salting-in, or increasing the solubility, of *p*-NP.[41, 53] Lithium chloride was found to increase SHG intensity denoting salting-out of *p*-NP, increasing the magnitude of free energy of adsorption of *p*-NP for the air/aqueous interface.[41] This information

allowed for an intriguing mode of inquiry for determining the effects on orientation and adsorption of *p*-$NP^-$ at the air/aqueous interface.

Electrolyte solutions have also been studied in terms of their surface potential. As electrolyte concentration is increased the surface potential of water changes.[54-55] It has been shown that when increasing concentrations of sodium chloride (NaCl) and sodium bromide (NaBr) the surface potential of water changes with a negative sign.[55] This negative sign change of the surface potential denotes the anions are closer to the interfacial region than the cations.[55] The structure of these ions within solution creates an electric double layer.[54-55] The electric double layer and the structure of the ions at the air/aqueous interface has an effect on the surface tension of the solution.[54] The surface potential of the air/aqueous interface is present because the electronic makeup between the air and aqueous phase are disparate.[44] Because *p*-$NP^-$ adsorbs to the air/aqueous interface it was expected that the double layer of anions and cations could affect the orientation of *p*-$NP^-$ at this surface.

## 4.2 Effect of Sodium Chloride on *p*-$NP^-$ at the Air/Aqueous Interface

Investigation of *p*-$NP^-$/electrolyte solutions began with NaCl. These solutions were made with *p*-NP crystal, NaCl, Millipore water made basic, (pH 13), with sodium hydroxide. As described in Chapter 3, glassware and sample dishes were prepared using aqua regia and soaked for 30 minutes. The sample dishes used were the same as stated in chapter 3 and dimensions can be referenced in figure 3.3. After exposure to aqua regia, glassware and dishes were rinsed 20 times with de-ionized water and then again 3 times with Millipore water. The *p*-$NP^-$ samples of 50mL in the corresponding electrolyte solution were placed into prepared Teflon dish and allowed to equilibrate for 15 minutes before measurement. This preparation is the same for all electrolytic experiment found within chapter 4.

Investigation of *p*-$NP^-$ at the air/aqueous interface of 1M and 2.5M NaCl solutions were performed and anisotropy data collected. Because of salt effects we found the the solubility of *p*-$NP^-$ in water decreased. Solutions of 1M NaCl and *p*-$NP^-$ were explored from concentrations of 5mM to 75mM. Due to decreased solubility 2.5 M NaCl solutions were examined from concentrations of *p*-$NP^-$ ranging from 4mM to 30mM. Electrolyte anisotropy data was analyzed with equations 2.5 and 2.6 and the Fresnel coefficients used to describe the penetration of electromagnetic energy into the interface are shown in table 4.1 below, like the case of the neat air/aqueous interface.

**Table 4.1** Fresnel Coefficients for fit equations with regards to *p*-$NP^-$, electrolyte solution air/aqueous interface

| $a_1$ | $a_2$ | $a_3$ | $a_4$ | $a_5$ |
|---|---|---|---|---|
| 0.170220943 | -0.19067986 | 0.094537194 | 0.160442965 | 0.170372194 |

These coefficients were solved assuming the electrolytic solution's refractive index was not significantly different than that of the non-electrolyte solutions analyzed within previous *p*-$NP^-$ work within the group. Refractive indices of electrolyte solutions has been investigated previously and did minimally deviated from the index of water, making our approximation appropriate.[56] Representative anisotropy data of both 1M and 2.5M NaCl solutions of *p*-$NP^-$ are included in figure 4.1 below. Within this figure, characteristic p-out and s-out data along with fit lines can be seen. Figure 4.1(a) and Figure 4.1(b) depict curve fit s-out and p-out low concentration *p*-$NP^-$ anisotropy data respectively. Anisotropy data for low concentration *p*-$NP^-$ solutions can be viewed with respect to anisotropy data in figure 3.5. The features of the curves are identical. Selected high concentration *p*-$NP^-$ solutions are represented by the data found in figure 4.1(c) and

figure 4.1(d). Within the p-out anisotropy graph, figure 4.1(d), the features have changed. However, s-out data found in figure 4.1(c) has the same characteristic features.

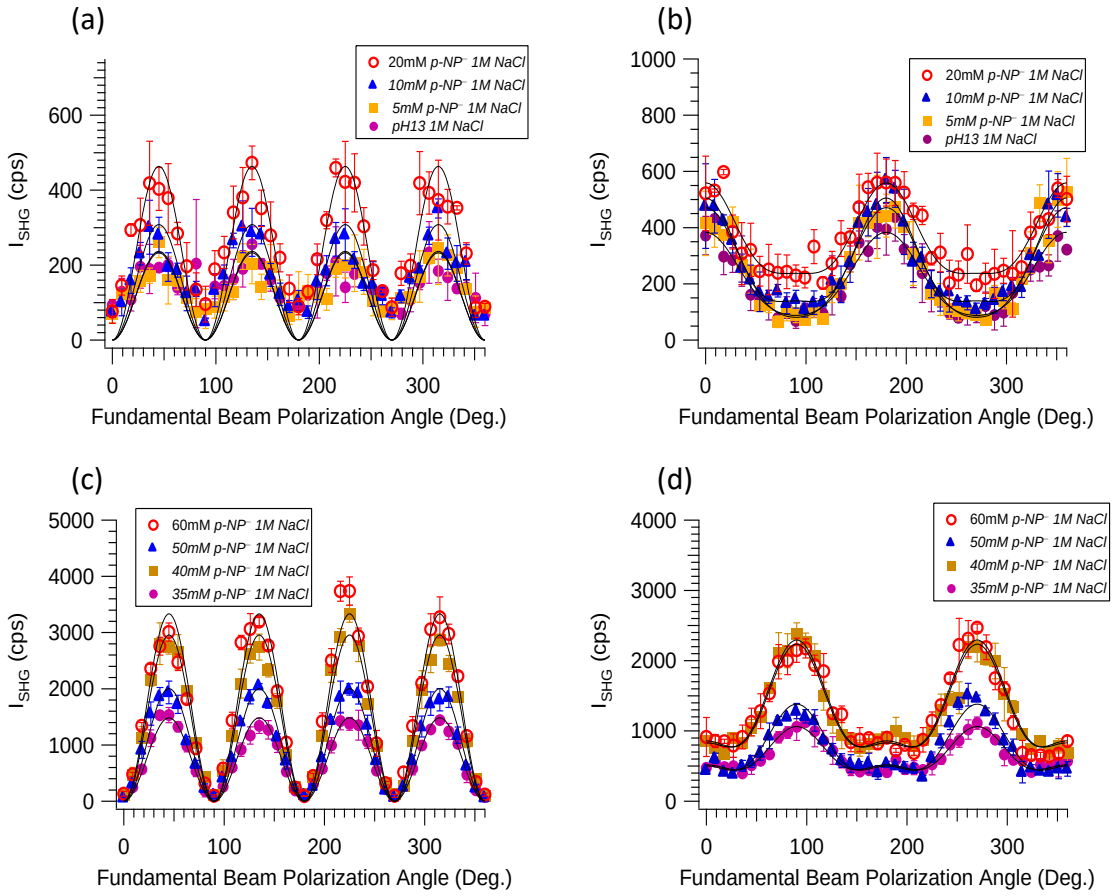


**Figure 4.1** (a) S-Out polarization data low concentration *p*-$NP^-$ 1M NaCl, (b) P-Out polarization data low concentration *p*-$NP^-$ 1M NaCl, (c) S-Out polarization data high concentration *p*-$NP^-$ 1M NaCl, (d) P--Out polarization data high concentration *p*-$NP^-$ 1M NaCl

Changing features within these graphs are evidence that the $\chi_{ijk}^{(2)}$ values are changing. This change can be a function of the surface population or a change in orientation, evident by equation 2.2. Susceptibilities were then analyzed using equation 2.7. Orientation of *p*-$NP^-$ with respect to the surface normal for 1M and 2.5M NaCl solutions are presented in figure 4.2. 1M NaCl solutions

show a *p*-NP⁻ orientation ranging from ca. 35° to ca. 55°. Comparing 2.5M NaCl solutions to 1M NaCl solutions one can see an even greater change in the angle of orientation of *p*-NP⁻ at the air/aqueous interface. The change in orientation at 2.5M NaCl changes from ca. 40° to over 60°.

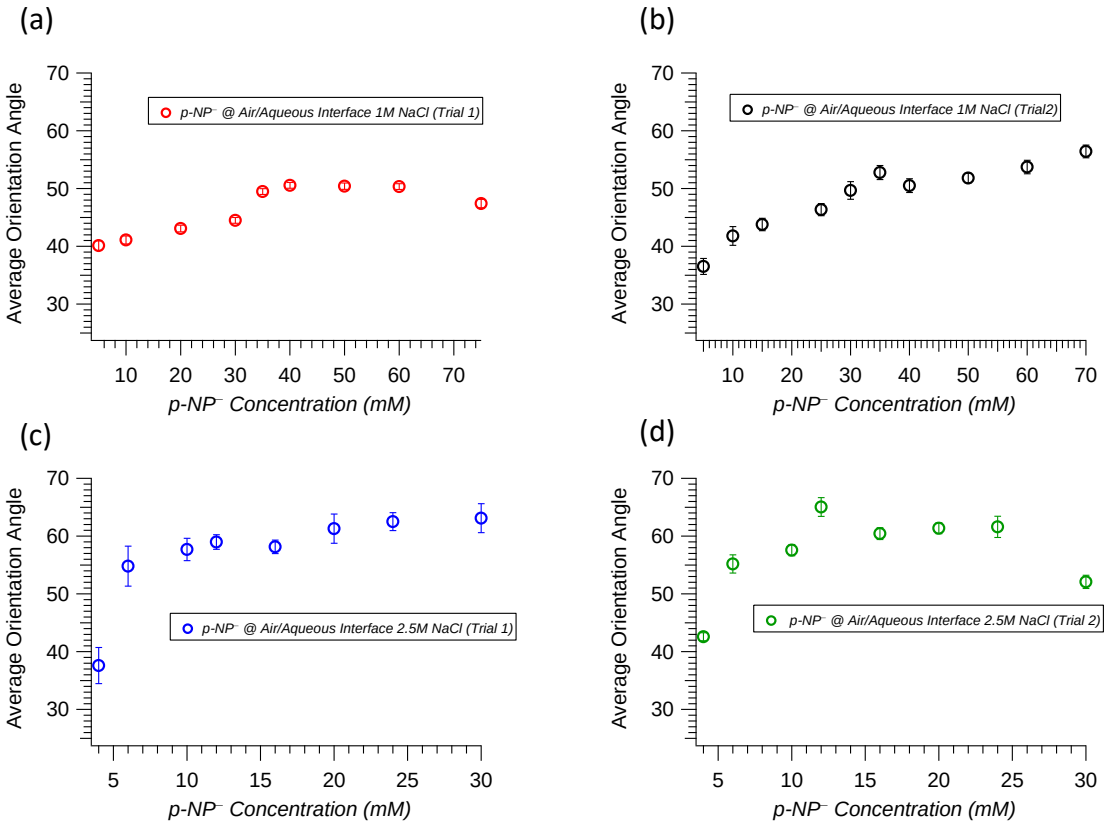


**Figure 4.2** Trials 1&2 for angles of orientation of *p*-NP⁻ at air/aqueous for 1M NaCl (a & b), Trials 1&2 for angles of orientation of *p*-NP⁻ at air/aqueous 2.5M NaCl solutions (c & d)

We find that the degree of change of the orientation of *p*-NP⁻ with respect to the surface normal is more pronounced with increasing concentration of sodium chloride. Expectations for data were that the cations within the electrolyte solutions would stabilize the orientation angles of *p*-NP⁻ at the air/aqueous interface thus eliminating variation of the orientation angle as a function of surface population. This expectation was centered on the structure of electrolyte solutions

making electric double layers.[54-55] Referring to figure 4.2, it is apparent that increasing concentration of electrolytes increase the degree to which *p*-$NP^-$ orientation is augmented. Shown in figure 4.3 the average orientation of *p*-$NP^-$ can be seen at air/aqueous interfaces of 0M, 1M, and 2.5M NaCl solutions. This distinctly shows the effect NaCl has upon the orientation of *p*-$NP^-$ at the air/aqueous interface, showing increased concentration leading to increased degree of change.

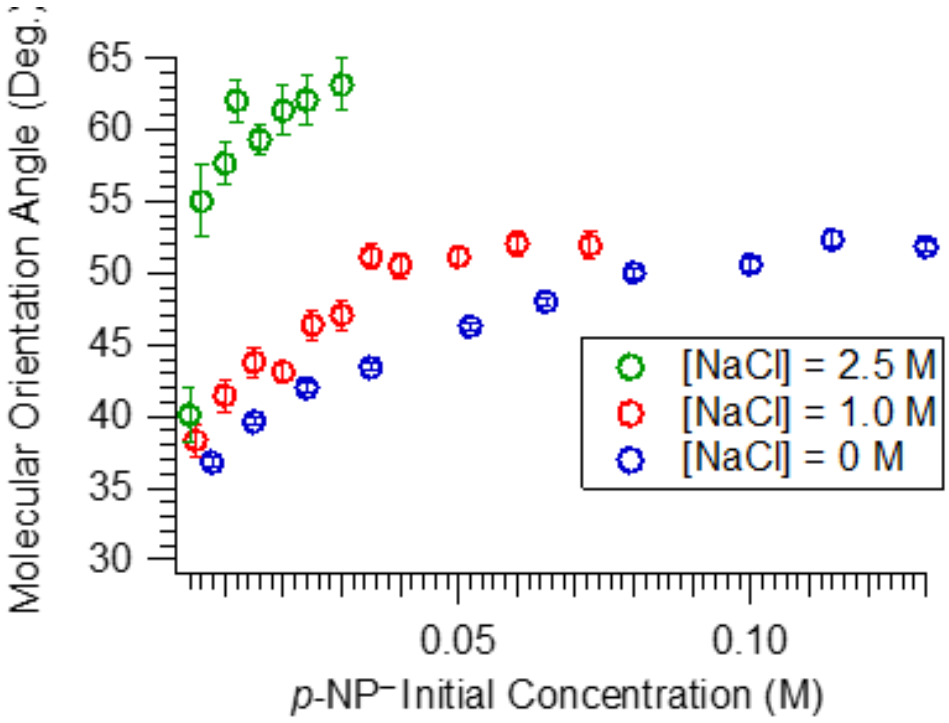


**Figure 4.3** Average angle of orientation of *p*-$NP^-$ at the air/aqueous interface for solutions with 0M, 1M, and 2.5 M NaCl.

To complement orientation data, it was necessary to do surface tensiometry measurements to determine the interfacial population of *p*-$NP^-$ within NaCl solutions. Data from the surface tension measurements, collected in our group, show the area per molecule of *p*-$NP^-$ at the interface. These values along with, Gibbs free energy of adsorption obtained using SHG and surface

tensiometry are reported in Table 4.2. Shown in figure 4.4 the area per molecule of *p*-$NP^-$ is graphed as a function of concentration (left axis). Comparison of figure 4.3 and figure 4.4 shows that as the space between *p*-$NP^-$ molecules decreases the orientation of these molecules increases.

**Table 4.2** Comparison of the free energy of adsorptions solved using Langmuir isotherm approximation for SHG and Surface Tensiometer data shown over range of electrolyte concentration. Maximum area per molecule found for saturated *p*-$NP^-$ solutions.

| **Electrolyte Concentration (M)** | $\Delta G_{ads}$ **(SHG) (kJ/mol)** | $\Delta G_{ads}$ **(Tensiometer) (kJ/mol)** | $Max.Area/molecule$ **(Tensiometer)** $(Å^2/molecule)$ |
|---|---|---|---|
| 0 | $-15.9 \pm 0.5$ | $-14.1 \pm 0.1$ | $144 \pm 4$ |
| 1.0 | $-16.4 \pm 0.7$ | $-15.5 \pm 0.1$ | $117 \pm 3$ |
| 2.5 | $-20.8 \pm 0.9$ | $-19.8 \pm 0.1$ | $272 \pm 9$ |

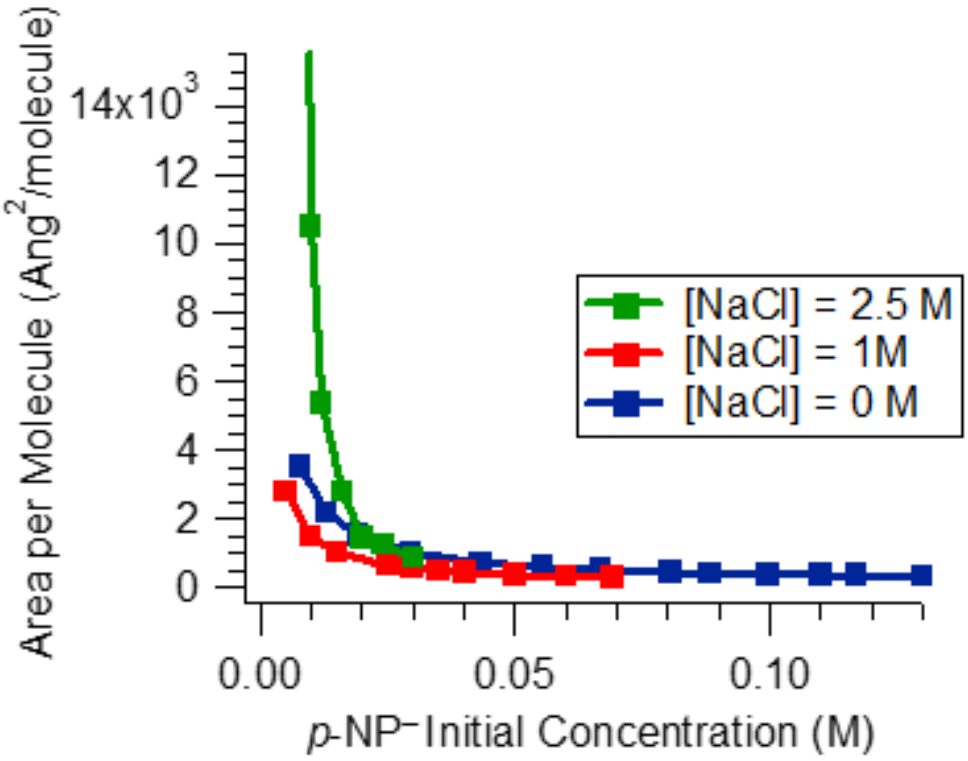


**Figure 4.4** Average area occupied by *p*-NP$^-$ at air/aqueous interfaces of solutions as a function of surface population of 0M, 1M, and 2.5M NaCl.

Reviewing the literature, we found evidence of halide presence at the air/aqueous interface.[8, 57-58] These polarizable anions are able to adsorb to the air/aqueous interface as determined by sum-frequency generation and molecular dynamics experiments.[8, 57-58] Larger halide ions were found to have greater affinity for the surface but chloride was also found to be present at the interface.[8, 57-58] Presented in table 4.3 are the molecular dynamic results for relative surface concentration of 1.2M sodium halide solutions.[8] This data shows chloride to have a large propensity for the air/aqueous interface with bromide and iodide having enhanced concentration

at the interface.[8] Table 4.3 also shows that the less polarizable sodium ion is relatively absent from this interface.[8]

**Table 4.3** – Relative concentrations of ions at air/aqueous interface with respect to the bulk concentration; via Molecular Dynamic Simulation.[8] Polarizabilities of the selected anions; reported in Å$^3$.[59]

| | Relative Concentration | | |
|---|---|---|---|
| **Solution** | **$Na^+$** | **$X^-$** | **$X^-$ polarizability (Å$^3$)** |
| NaF | 0.16 | 0.07 | 1.20 |
| **NaCl** | **0.16** | **0.71** | **3.65** |
| **NaBr** | **0.81** | **2.10** | **4.96** |
| NaI | 0.69 | 2.91 | 7.30 |

## 4.3 Effect of Sodium Bromide on *p*-$NP^-$ at the Air/Aqueous Interface

To substantiate the interaction of chloride ion at the air/aqueous interface investigation of sodium bromide (NaBr) solutions was therefore pursued. Due to enhancement of bromide at the air/aqueous interface it was expected to see the orientation of *p*-$NP^-$ would increase with respect to the surface normal. To explore this interaction, 1M and 2.5M NaBr solutions were analyzed with the same preparation and *p*-$NP^-$ concentration range as the NaCl experiments.

Anisotropy data of NaBr solutions showed the same features displayed in figure 4.1. Higher concentrations of *p*-$NP^-$ displayed a change in feature of the graph indicative of changing susceptibility. These susceptibilities were solved for using equations 2.5 and 2.6. The Fresnel coefficients used to describe the penetration of electric field into the interface were assumed to be the same as those for the NaCl experiments, found in table 4.1. Upon solving for the susceptibilities, the ratio between them could be analyzed using equation 2.7 and the average

orientation angle with respect to the surface normal could be deduced. In figure 4.5 the average orientation of *p*-NP$^-$ at the air/aqueous interface of NaBr solutions is shown. Representative data from experiments of 1M and 2.5M NaBr and a comparison of 1M NaCl and 1M NaBr of *p*-NP$^-$ are presented within figure 4.5. The angle of *p*-NP$^-$ about the surface normal increases as surface population increases, similar to the NaCl experiments. The degree to which the angle of *p*-NP$^-$ changes ranges from ca. 35° to ca. 60° for 1M NaBr and 2.5 M NaBr. Referring to figure 4.5 it can be seen the degree of change of *p*-NP$^-$ orientation for 1M NaBr solutions is comparable to 1M NaCl solutions but greater. This provides evidence that polarizable anions influence the orientation of *p*-NP$^-$ at the air/aqueous interface.

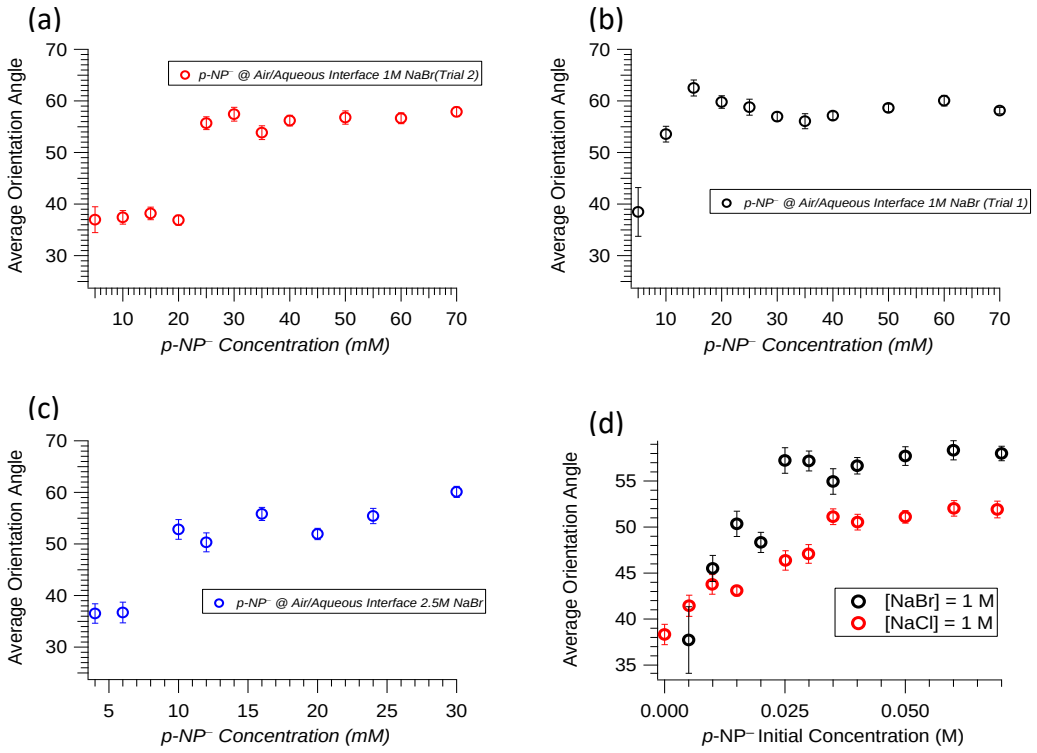


**Figure 4.5** Representative Orientation data for *p*-NP$^-$ at the air aqueous interface of 1M NaBr solutions (a) and 2.5M NaBr solutions (b). Comparison of orientation of *p*-NP$^-$ at the air/aqueous interface between 1M NaCl and 1M NaBr solutions (c).

## 4.4 Adsorption Isotherm of *p*-$NP^-$ within Electrolyte Solutions

Adsorption isotherm analysis of the electrolyte data was also performed. Using equation 3.1 the data collected for NaCl and NaBr solutions could be interpreted and plotted against *p*-$NP^-$ concentration to yield an isotherm. The orientation insensitive angle calculated using equation 3.2 was found to be 61°. Isotherm data shown in figure 4.6 reveal that the Langmuir isotherm assumption holds for *p*-$NP^-$ adsorption in different electrolytic media. The data were fit using equation 2.11. The free energy of adsorption was solved for using equation 2.12 and can be seen in table 4.2. The free energy of adsorption calculated using SHG measurements and surface tensiometer measurements are within agreement, lending evidence that the Langmuir model was appropriate. It can be seen the magnitude of free energy of adsorption of *p*-$NP^-$ increases from 0 to 2.5M NaCl. However, the distance between *p*-$NP^-$ species, for maximum surface coverage, decreases from 0 to 1M but is greater than either at 2.5M NaCl concentration. This is possibly because of the presence at the air/aqueous interface the change in free energy of *p*-$NP^-$ from 1M to 2.5M NaCl solutions may be due to competition for surface sites.[8]

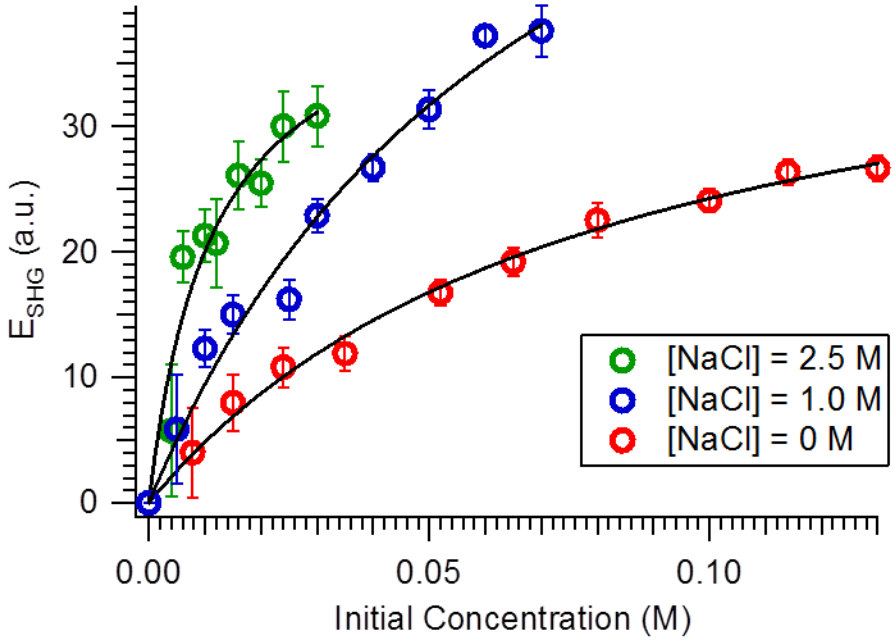


**Figure 4.6** Adsorption Isotherm of *p*-$NP^-$ in 0M, 1M, and 2.5M NaCl solutions

Electrolyte data was collected and analyzed with the aim of understanding the change of *p*-$NP^-$ at the neat air/aqueous interface. With the experimental evidence presented, now we turn to Chapter 5, where physical interpretation of DPPC and electrolytic data can be offered to describe phenomenon put forth within Chapters 2 and 3.

# Chapter 5 – Discussion, Future Direction, and Concluding Remarks

It has been shown that the adsorption and variation of *p*-$NP^-$ orientation is dependent on the different solution and interfacial environments. To recap, the air/aqueous interface has been shown to be a dynamic environment and its effects upon *p*-$NP^-$ have been investigated with the focus on adsorption and orientation. Herein, we discuss the physical insights obtained and their implications, specifically with respect to the ultimate goal of understanding the reactivity of *p*-$NP^-$ at the interfacial region.

## 5.1 Interpretation of Experimental Results

We have shown DPPC monolayer does restrict the orientation of *p*-$NP^-$ at the air/aqueous interface. The angle of orientation of *p*-$NP^-$ about the surface normal was shown to be 30° ca. and invariant as a function of surface population. This is evidence that molecular interactions at the air/aqueous interface have the ability to alter orientation. The fact that this angle matches closely to previous investigation of DPPC tail orientation (25°) maybe evidence that *p*-$NP^-$ is embedded within the DPPC monolayer, as shown in figure 3.6.[33] It was evident that there were forces causing *p*-$NP^-$ orientation at the unaltered air/aqeuous interface to change as surface population increased. This was in contrast to an unaffected neutral *p*-NP at the air/aqueous interface.[7] Although source of this change was not elucidated via restriction of DPPC, it can be seen that the magnitude of molecular interaction between DPPC and *p*-$NP^-$ at the air/aqueous interface is indeed greater than the magnitude of the force altering *p*-$NP^-$ orietation at an unaltered interface.

Electrolyte solutions were interesting in the unexpected results obtained. Understanding the electorlytic solutions, which form double layers, that tend to neutralize charge at the interfacial region lead us to believe cations would play a role in *p*-$NP^-$ orientation at this air/aqueous

interface.[54-55] It was expected that sodium ions would possibly diminish the *p*-$NP^-$ angle change if indeed the source of this change was coulombic in nature. The opposite was found to be true; *p*-$NP^-$ at the air/aqueous interface of electrolyte solutions underwent a greater degree of change as surface population increased than found for solutions with negligible ionic stength.

Intriguingly enough, studies have shown polarizability of halide anions allow for their adsorption to the air/aqueous interface.[8, 57-58] Coulombic interaction between these adsorbed halide anions and *p*-$NP^-$ could then be deduced as the source of orientation change within the electrolyte solutions. Referring to table 4.2 it can be seen that within NaCl solutions, the free energy of adsorption for *p*-$NP^-$ at the air/aqueous interface increases as NaCl concentration increases. This was to be expected due to salting-out effects, explored previously within other studies.[41, 53] However, competetion between surface adsorbed species, such as chloride and *p*-$NP^-$, result in surface population variation that is not linearly dependent upon NaCl concentration. Necessarily, table 4.2 and the data regarding distance between *p*-$NP^-$ molecules must be considered when establishing the source of orientation change at this interface. When doing so it can be seen that the distance between *p*-$NP^-$ molecules is greater (~1.4 nm) than can be accounted for by clear coulombic interaction between *p*-$NP^-$ molecules. Electrolytes have the ability to enhance this effect and other surface adsorbed species can influence the angle of *p*-$NP^-$ at the interface. Intuitively, orientation of *p*-$NP^-$ should change with interaction with other surface adsorbed species. This may elucidate possible source of orientation change of *p*-$NP^-$ as a function of surface population at the neat air/aqueous interface. Interaction between an electron rich *p*-$NP^-$ and the solvent water molecules may have been the source of this change at the neat air/aqueous interface.

Studies have been done that suggest hydroxide may adsorb to the oil/water interface.[60-61] Our investigations of *p*-$NP^-$ have been done at pH 13 to ensure isolation of this species. This high

concentration of hydroxide may lead to surface adsorbed hydroxide that in turn interact with *p*-$NP^-$ at the air/aqueous interface resulting in the change in orientation. However, studies have also suggested that hydroxide ion is not present at the air/aqueous interface.[62-63] Therefore, the effect of hydroxide ion on orientation of *p*-$NP^-$ at the air/aqueous interface is inconclusive.

Solutions containing NaBr confirm the analysis that halide ion indeed is affecting the orientation of *p*-$NP^-$ at the air/aqueous interface. According to computational studies, bromide is found to be enhanced at the interfacial region compared to the bulk solution.[8] Table 4.3 shows that bromide is more polarizable than chloride and so is more likely to adsorb to the air/aqueous interface. Our examination of *p*-$NP^-$ agrees with this conlusion. The degree to which *p*-$NP^-$ changes orientation is indeed increased from the introduction of NaBr compared to NaCl within 1M concentrations. The effect on surface population of NaBr has yet to be examined through surface tension measurements and because the surface population of *p*-$NP^-$ maybe varied to a degree that would not allow a side by side comparison of orientation data between of 2.5M NaBr and NaCl solutions. Seen in table 4.2 the area per molecule of *p*-$NP^-$ at the air/aqueous interface is actually greater for 2.5M NaCl solutions and the same trend may be increased considering bromide's affinity for this region.

## 5.2 Plausible Future Experiments

Future investigation could build upon both restriction and enhancement of the orientation angle of *p*-$NP^-$ at the interface. Regarding the restriction of *p*-$NP^-$ at the air/aqueous interface it would be beneficial to perform Langmuir trough experiments to determine the exact surface population of DPPC monolayers. In addition, trying lipids of varying chain lengths may have intriguing results. Is there a tail chain length that fails to restrict *p*-$NP^-$? What could this mean about the magnitude of the interaction affecting *p*-$NP^-$ orientation at the surface? Would longer

chains result in different orientation angles of *p*-$NP^-$ at the interface? Varying the lipids would also allow us to probe if *p*-$NP^-$ orientation is indeed linked to chain tilt at the interface. In addition to focusing upon the chains of the lipids various head groups could be investigated to determine how adsorption and orientation of *p*-$NP^-$ is affected. Using positive or negatively charged groups would seem to have a straightforward affect on the adsorption of *p*-$NP^-$ to this interface. It would also allow for better understanding of the role of the solvated head group in the orientation of *p*-$NP^-$ at the interface.

The future direction for electrolyte experiments needs to focus upon getting surface tension measurements on the NaBr solutions already investigated within this work. This would allow for a full analysis of the interactions occuring with *p*-$NP^-$ at this interface. Because electrolyte solutions have been shown to form electric double layers it would be interesting to pursue investigation of various cations to determine the role they play in adsorption and orientation of *p*-$NP^-$ at the air/aqueous interface. It could also be interesting to pursue the salting-in agents investigated previously to find how the orientation of *p*-$NP^-$ is affected.[53] Salting-in agents, such as guandinium chloride are positively charged and could give more insight upon the role of cations within this discussion.

## 5.3 Photo-Degradation of *p*-$NP^-$ at the Air/Aqueous Interface

Ultimately the goal in investigation of interfacial *p*-$NP^-$ is to understand reactivity in this unique environment. Photo-degradation of *p*-$NP^-$ has been investigated within our group. In these investigations *p*-$NP^-$ has been shown to remain undegraded after more than 400 minutes of UV exposure.[7] This was in contrast to bulk measurements that was reduced by nearly 15% over the same time period. One factor that made the surface photo-chemistry study difficult is the long degradation time.

In order to examine the photo-reactivity of *p*-$NP^-$ at the air/aqueous interface it was necessary to speed the reaction. Comparison of the affects of hydrogen peroxide ($H_2O_2$) on photo-degradation of *p*-$NP^-$ in the bulk and air/aqueous interface was done. The experimental setup for this experiment was done previously in our group and described earlier.[7] Several concentrations of $H_2O_2$ were examined for bulk degradation of *p*-$NP^-$ solutions. Results show significant rate increases with the addition of $H_2O_2$ with a maximum affect at 9mM. Beyond this concentration $H_2O_2$ may be self-reacting and lowering its effective concentration upon which it will react with *p*-$NP^-$ in solution.

To complement this bulk photolysis, investigation of *p*-$NP^-$ photo-degradation at the air/aqueous interface in solution with $H_2O_2$ has begun. Control experiment, with no UV degradation, 18mM $H_2O_2$, in a pH 13 solution of 130mM *p*-$NP^-$ has been performed. In addition, one trial has been collected with the concentrations of *p*-$NP^-$ and $H_2O_2$ described in the control with UV exposure of 240 minutes. Both the control and degraded experiments are shown in figure 5.1(a). A sample were prepared using *p*-NP crystal dissolved within pH13 Millipore water. Stock solution of 900mM $H_2O_2$ was made from Fisher Chemical purchased $H_2O_2$ (H323-500, Certified 30%) and dissolved within Millipore water. Before experimentation 98mL of 130mM *p*-$NP^-$ was prepared with 2mL of 900mM $H_2O_2$ to produce a final 18mM $H_2O_2$ , 130mM *p*-$NP^-$ solution.

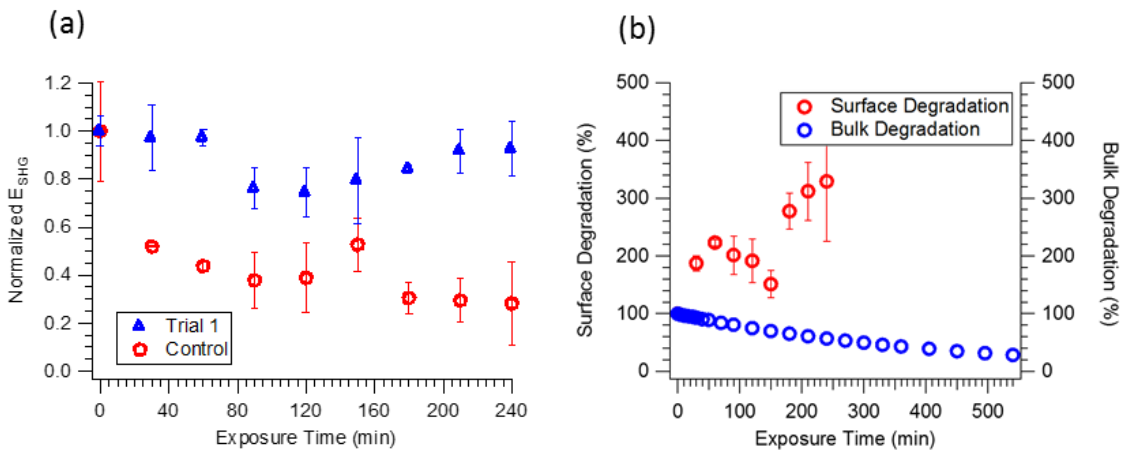


**Figure 5.1** (a) 130mM *p*-$NP^-$ solutions with 18mM $H_2O_2$ measured for SHG intensity every 30 minutes over the course of 240 minutes. Control in red had no UV exposure while Trial 1 in blue was exposed to UV light during this time period. (b) Normalized photo-degradation experiments of 18mM $H_2O_2$, 130mM *p*-$NP^-$ for bulk (blue) and surface (red). The bulk degradation data was collected by Ms. Margret Schimts in our group.

In figure 5.1(a), we see that SHG intensity corresponding to control experiment, decreases during the 240 minute time period. Because the second harmonic field is proportional to the surface population of adsorbed species, as seen in equation 2.2, this denotes loss of *p*-$NP^-$ at this interface without UV exposure. In contrast, UV exposure of the experimental solutions (blue) has relatively no loss in SHG intensity over the course of 240 minutes. Results of these surface experiments are in stark contrast to those performed on the bulk solution. Figure 5.1(b) shows normalized experiments of 18mM $H_2O_2$ bulk and surface degraded *p*-$NP^-$ solutions. Due to the change in SHG intensity of *p*-$NP^-$ within the control and no change in intensity during UV exposure, figure 5.1(b) shows an positive slope. Bulk degradation was able to be analyzed and degradation of *p*-$NP^-$ occurred as expected, evidence that $H_2O_2$ does not affect the concentration of *p*-$NP^-$ within the bulk solution in the case of concentrations ranging from 4.5mM to 18mM. Interestingly, in the

case of the control experiment due to the decrease in SHG signal, denoting removal of *p*-$NP^-$ surface, it can be concluded that $H_2O_2$ is interacting w/ the surface bound *p*-$NP^-$. The exact interaction of $H_2O_2$ with *p*-$NP^-$ cannot be concluded with SHG measurement but $H_2O_2$ surface propensity is intriguing. These preliminary results highlight the unique influence of the interface on chemical reactions.

Future work can be done to elucidate the effect of the air/aqueous interfacial environment on *p*-$NP^-$ photolysis. Varying concentration of $H_2O_2$ could allow determination of a solution that has no effect on SHG intensity over control investigation. Surface pH may be a contributing factor in the decrease of SHG signal. If possible atmospheric control during experimentation may allow for elimination of acidification and allow for a concrete examination of photolysis of *p*-$NP^-$ at the air/aqueous interface in presence of $H_2O_2$. It may also be necessary to vary concentration of *p*-$NP^-$ to limit change during the control experiment. Examining, the effects of environments of electrolyte or lipid monolayers could provide many insights to surface photo-degradation of *p*-$NP^-$ solutions. It is of direct importance to begin with adequetly describing *p*-$NP^-$ photolysis without alteration before adding variables.

## 5.4 Concluding Remarks

Interfacial chemistry investigated with SHG has proven to be a challenging and rewarding endeavor. The systems of *p*-$NP^-$ at several air/aqueous interfacial environments, provided many opportunites to grasp at fundamental nature of ions, both oraganic and inorganic at the solution surface. This knowledge has application within environmental chemistry and the system is far from completely understood. This thesis, however, succesfully added to the overall study of organic ions and particularly *p*-$NP^-$ activity at the air/aqueous interface.

# References


1. Bacon, F.; Fowler, T., *Novum organum*. 2nd edition, corrected and reviewed ed.; Clarendon Press: Oxford, 1889.
2. Locke, J., *An Essay Concerning Human Understanding*. Dover Publications: New York :, 1959.
3. Lear, G. R., *Happy Lives and the Highest Good*. Princeton University Press: United States, 2004.
4. Aquinas, S. T., *Commentary on the Posterior Analytics of Aristotle*. Hamilton Printing Co.: Rensselar, New York, 1970.
5. Onsager, L.; Samaras, N. N. T., The Surface Tension of Debye-Huckel Electrolytes. *The Journal of Chemical Physics* **1934,** *2* (8), 528-536.
6. Rao, Y.; Subir, M.; McArthur, E. A.; Turro, N. J.; Eisenthal, K. B., Organic Ions at the Air/Water Interface. *Chemical Physics Letters* **2009,** *477* (4-6), 241-244.
7. Headly, D. Equilibrium and Photokinetic Properties of Phenolic Compounds at the Air-Water Interface. Ball State University, 2016.
8. Jungwirth, P.; Tobias, D. J., Molecular Structure of Salt Solutions: A New View of the Interface with Implications for Heterogeneous Atmospheric Chemistry. *The Journal of Physical Chemistry B* **2001,** *105* (43), 10468-10472.
9. Tamburello-Luca, A. A.; Hebert, P.; Brevet, P. F.; Girault, H. H., Resonant-Surface Second-Harmonic Generation Studies of Phenol Derivatives at Air/Water and Hexane/Water Interfaces. *Journal of the Chemical Society, Faraday Transactions* **1996,** *92* (17), 3079-3085.
10. Atkins, P.; Paula, J. d., *Physical Chemistry*. 8th ed.; Macmillan: New York, NY, 2010.
11. Eisenthal, K. B., Liquid Interfaces Probed by Second-Harmonic and Sum-Frequency Spectroscopy. *Chemical Reviews* **1996,** *96* (4), 1343-1360.
12. Geiger, F. M., Second Harmonic Generation, Sum Frequency Generation, and chi((3)): Dissecting Environmental Interfaces with a Nonlinear Optical Swiss Army Knife. *Annual Review of Physical Chemistry* **2009,** *60*, 61-83.
13. Sørensen, B., *A History of Energy: Northern Europe from Stone Age to the Present Day*. Earthscan: Abingdon, Oxon, 2012.
14. Mikhail, A., *Nature and Empire in Ottoman Egypt*. Cambridge University Press: New York, NY, 2011.
15. Steckel, R. A History of the Standard of Living in the United States. http://eh.net/encyclopedia/a-history-of-the-standard-of-living-in-the-united-states/ (accessed June 13).
16. Storey, G., *Charles Dickens, Bleak House*. Cambridge University Press: Cambridge [Cambridgeshire] ;, 1987.
17. US Environmental Protection Agency: Quality Criteria for Water. EPA, Ed. Washington, D.C., 1986.
18. Samuel, M. S.; Sivaramakrishna, A.; Mehta, A., Bioremediation of *p*-Nitrophenol by Pseudomonas putida 1274 Strain. *Journal of Environmental Health Science and Engineering* **2014,** *12* (1), 53-60.
19. Islam, S.; Bormon, S. K.; Nadim, M.; Hossain, K.; Habib, A.; Islam, T. S. A., Photocatalytic Degradation of p-Nitrophenol (PNP) in Aqueous Suspension of TiO2. *American Journal of Analytical Chemistry* **2014,** *05* (08), 483-489.
20. Nakagawal, M.; Crosb, D. G., Photodecomposition of Nitrofen. *Journal of Agriculture and Food Chemistry* **1974,** *22* (5), 849-853.
21. Nakagawal, M.; Crosby*, D. G., Photonucleophilic Reactions of Nitrofen. *Journal of Agriculture and Food Chemistry* **1974,** *22* (6), 930-933.
22. Agency for Toxic Substances and Disease Registry (ATSDR): Toxicological profile for nitrophenols; 2-nitro-phenol and 4-nitro-phenol. Services, U. S. D. o. H. a. H., Ed. Atlanta, USA, 1992.
23. Sigma-Aldrich *p*-Nitrophenol; SDS no. 1041 [Online]. http://www.sigmaaldrich.com/MSDS/MSDS/DisplayMSDSPage.do?country=US&language=en&pro

ductNumber=1041&brand=SIGMA&PageToGoToURL=http%3A%2F%2Fwww.sigmaaldrich.com%2Fcatalog%2Fproduct%2Fsigma%2F1041%3Flang%3Den (accessed April 13).

24. Mounib, M. S., Metabolism of Pyruvate Fish and Rabbits. *Comparative Biochemistry and Physiology* **1967,** *22*, 539-548.
25. Society, U. S. G. https://water.usgs.gov/edu/earthhowmuch.html (accessed November 19).
26. Knipping, E. M.; Lakin, M. J.; Foster, K. L.; Jungwirth, P.; Tobias, D. J.; Gerber, R. B.; Dabdub, D.; Finlayson-Pitts, B. J., Experiments and Simulations of Ion-Enhanced Interfacial Chemistry on Aqueous NaCl Aerosols. *Science* **2000,** *288*, 301-306.
27. Adams, E.; Allen, H., Palmitic Acid on Salt Subphases and in Mixed Monolayers of Cerebrosides: Application to Atmospheric Aerosol Chemistry. *Atmosphere* **2013,** *4* (4), 315-336.
28. Somorjai, G. A.; Li, Y., Impact of Surface Chemistry. *Proceedings of the National Academy of Sciences of the United States of America* **2011,** *108* (3), 917-924.
29. Mrksich, M., Mass Spectrometry of Self-Assembled Monolayers: A New Tool for Molecular Surface Science. *ACS Nano* **2008,** *2* (1), 7-18.
30. Kolb, C. E.; Worsnop, D. R., Chemistry and Composition of Atmospheric Aerosol Particles. *Annual Review of Physical Chemistry* **2012,** *64*, 471-491.
31. Bredenbeck, J.; Ghosh, A.; Niewnhuys, H.-K.; Bonn, M., Interface-Specific Ultrafast Two-Dimensional Vibrational Spectroscopy. *Accounts of Chemical Research* **2009,** *42* (9), 1332-1342.
32. Luca, A. A. T.; Hebert, P.; Brevet, P. F.; Girault, H. H., Surface Second-Harmonic Generation at Air-Solvent and Solvent-Solvent Interfaces. *Journal of the Chemical Society, Faraday Transactions* **1995,** *91* (12), 1763-1768.
33. Ma, G.; Allen, H. C., DPPC Langmuir Monolayer at the Air−Water Interface: Probing the Tail and Head Groups by Vibrational Sum Frequency Generation Spectroscopy. *Langmuir* **2006,** *22* (12), 5341-5349.
34. Simpson, G. J., New Tools for Surface Second Harmonic Generation. *Applied Spectroscopy Focal Point* **2001,** *55* (1), 16-32.
35. Corn, R. M.; Higgins, D. A., Optical Second Harmonic Generation as a Probe of Surface Chemistry. *Chemical Reviews* **1994,** *94*, 107-125.
36. Vidal, F.; Tadjeddine, A., SFG Spectroscopy of Interfaces. *Reports on Progress in Physics* **2005,** *68*, 1095-1127.
37. Boyd, R. W., *Non-Linear Optics*. 2nd Edition ed.; Academic Press: San Diego, Ca, 2003.
38. Brevet, P. F.; Girault, H. H., *Second Harmonic Generation at Liquid/Liquid Interfaces*. CRC Press: 1996.
39. Griffiths, D. J., *Introduction to Electrodynamics*. 3rd ed.; Prentice Hall: Upper Saddle River, New Jersey, 1999.
40. Moad, A. J.; Simpson, G. J., A Unified Treatment of Selection Rules and Symmetry Relations for Sum-Frequency and Second Harmonic Spectroscopies. *Journal of Physical Chemistry* **2004,** *108* (11), 3548-3562.
41. Das, K.; Sarkar, N.; Das, S.; Datta, A.; Nath, D.; Bhattacharyya, K., Salt Effect on *p*-Nitrophenol at the Water Surface: A Surface Second Harmonic Generation Study. *Journal of the Chemical Society, Faraday Transactions* **1996,** *92* (24), 4993-4996.
42. Higgins, D. A.; Abrams, M. B.; Byerly, S. K.; Corn, R. M., Resonant 2nd Harmonic-Generation Studies of *p*-Nitrophenol Adsorption at Condensed-Phase Interfaces. *Langmuir* **1992,** *8* (8), 1994-2000.
43. Shoemake, K., Animating Rotation with Quaternion Curves. *SIGGRAPH Comput. Graph.* **1985,** *19* (3), 245-254.
44. Myers, D., *Surfaces, Interfaces, and Colloids: Principles and Applications*. 2nd ed.; John Wiley & Sons Inc.: United States, 1999.

45. Hanaor, D. A. H.; Ghadiri, M.; Chrzanowski, W.; Gan, Y., Scalable Surface Area Characterization by Electrokinetic Analysis of Complex Anion Adsorption. *Langmuir* **2014,** *30* (50), 15143-15152.
46. Daubert, T. E.; Danner, R. P., *Physical and Thermodynamic Properties of Pure Chemicals Data Compilation*. Taylor and Francis: Washington D.C., 1989.
47. Dean, J. A., *Lange's Handbook of Chemistry*. McGraw-Hill: New York,N.Y., 1999.
48. Willingham, C. B.; Taylor, W. J.; Pignocco, J. M.; Rossini, F. D., Vapor Pressures and Boiling Points of Some Paraffin, Alkylcyclopentane, Alkylcyclohexane, and Alkylbenzene Hydrocarbons. *Journal of Research of the National Bureau of Standards* **1945,** *35* (3), 219-244.
49. Mohwald, H., Phospholipid and Phospholipid-Protein Monolayers at the Air/Water Interface. *Annual Review of Physical Chemistry* **1990,** *41*, 441-476.
50. Dominguez, H.; Smondyrev, A. M.; Berkowitz, M. L., Computer Simulations of Phosphatidylcholine Monolayers at Air/Water and CCl4/Water Interfaces. *The Journal of Physical Chemistry B* **1999,** *103* (44), 9582-9588.
51. Kienle, D. F.; de Souza, J. V.; Watkins, E. B.; Kuhl, T. L., Thickness and Refractive Index of DPPC and DPPE Monolayers by Multiple-Beam Interferometry. *Analytical and Bioanalytical Chemistry* **2014,** *406* (19), 4725-4733.
52. Simpson, G. J.; Rowlen, K. L., An SHG Magic Angle: Dependence of Second Harmonic Generation Orientation Measurements on the Width of the Orientation Distribution. *Journal of the American Chemical Society* **1999,** *121* (11), 2635-2636.
53. Sarkar, N.; Das, K.; Das, S.; Nath, D.; Bhattacharyya, K., Effect of Urea and Surfactant on *p*-Nitrophenol at the Water Surface: a Surface Second-Harmonic Generation Study. *Journal of the Chemical Society, Faraday Transactions* **1995,** *91* (12), 1769-1773.
54. Petersen, P. B.; Saykally, R. J., On the Nature of Ions at the Liquid Water Surface. In *Annual Review of Physical Chemistry*, Annual Reviews: Palo Alto, 2006; Vol. 57, pp 333-364.
55. Jarvis, N. L.; Scheiman, M. A., Surface Potentials of Aqueous Electrolyte Solutions. *Journal of Physical Chemistry* **1968,** *72* (1), 74-78.
56. Tan, C.-Y.; Huang, Y.-X., Dependence of Refractive Index on Concentration and Temperature in Electrolyte Solution, Polar Solution, Nonpolar Solution, and Protein Solution. *Journal of Chemical & Engineering Data* **2015,** *60* (10), 2827-2833.
57. Piatkowski, L.; Zhang, Z.; Backus, E. H. G.; Bakker, H. J.; Bonn, M., Extreme surface propensity of halide ions in water. *Nature Communications* **2014,** *5*.
58. Ishiyama, T.; Morita, A., Molecular Dynamics Study of Gas−Liquid Aqueous Sodium Halide Interfaces. II. Analysis of Vibrational Sum Frequency Generation Spectra. *The Journal of Physical Chemistry C* **2007,** *111* (2), 738-748.
59. Coker, H., Polarizability Changes on Ion Hydration. *The Journal of Physical Chemistry* **1976,** *80* (19), 2084-2091.
60. Fang, H.; Wu, W.; Sang, Y. J.; Chen, S. L.; Zhu, X. F.; Zhang, L. B.; Niu, Y. Y.; Gan, W., Evidence of the Adsorption of Hydroxide Ion at Hexadecane/Water Interface from Second Harmonic Generation Study. *Rsc Advances* **2015,** *5* (30), 23578-23585.
61. Creux, P.; Lachaise, J.; Graciaa, A.; Beattie, J. K., Specific Cation Effects at the Hydroxide-Charged Air/Water Interface. *The Journal of Physical Chemistry C* **2007,** *111* (9), 3753-3755.
62. Petersen, P. B.; Saykally, R. J., Probing the Interfacial Structure of Aqueous Electrolytes with Femtosecond Second Harmonic Generation Spectroscopy. *The Journal of Physical Chemistry B* **2006,** *110* (29), 14060-14073.
63. Vácha, R.; Rick, S. W.; Jungwirth, P.; de Beer, A. G. F.; de Aguiar, H. B.; Samson, J.-S.; Roke, S., The Orientation and Charge of Water at the Hydrophobic Oil Droplet–Water Interface. *Journal of the American Chemical Society* **2011,** *133* (26), 10204-10210.